Supplementary Data

Supplementary Figure S1. Platinum compound concentrations and uptake.

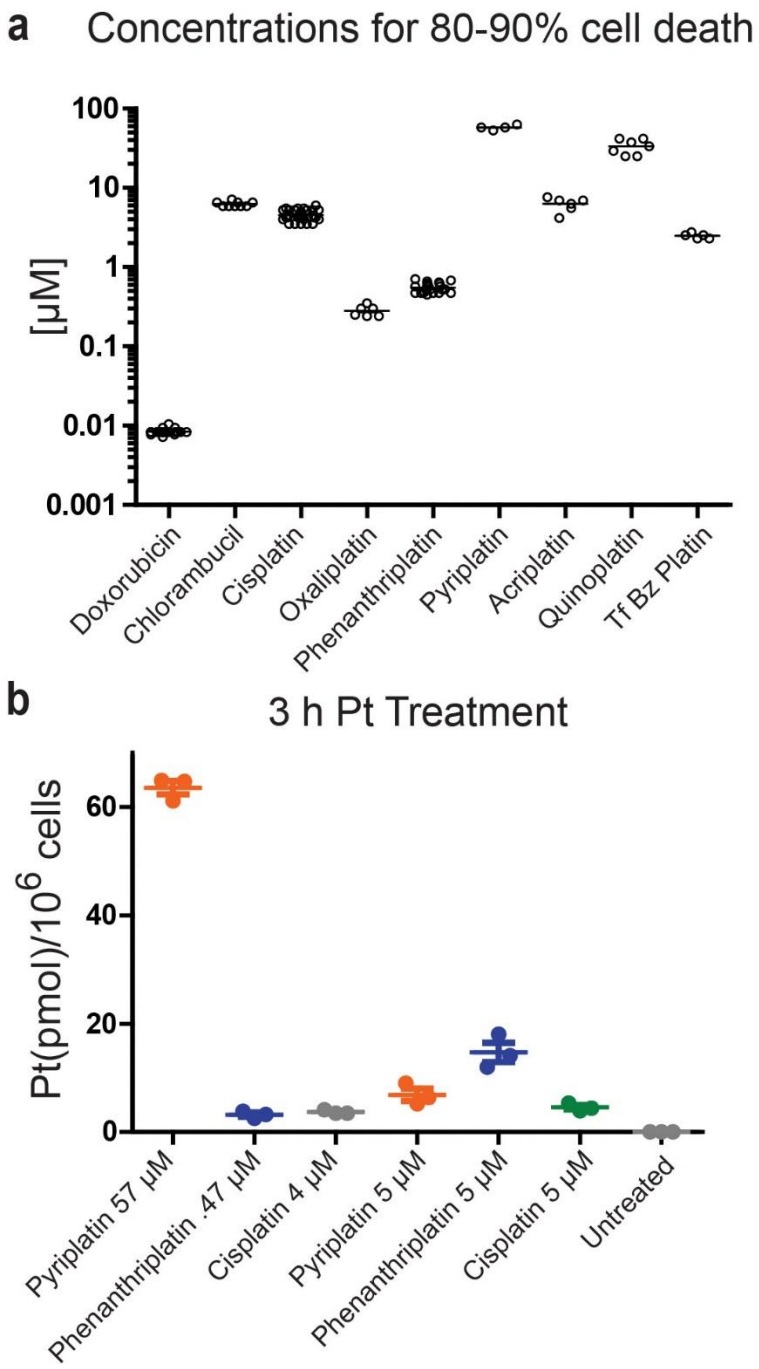

(**a**) Concentrations used to achieve 80-90% cell death in *Eμ-Myc p19*$^{Arf-/-}$ lymphoma cells for several platinum compounds as well as doxorubicin and chlorambucil. Doses were conducted on at least three distinct thaws of cells. N is listed from left to right as shown above: 25, 9, 30, 6, 24, 4, 6, 7 and 5. (**b**) Cellular uptake of platinum over a 3 h incubation period in *Eμ-Myc p19*$^{Arf-/-}$ lymphoma cells presented in units of pmol of Pt per 10^6 cells. Conducted from three independent cell cultures and doses. Error bars represent mean ± SEM.

Supplementary Figure S2. RNAi signatures identify a spectrum of activities among platinum analogues.

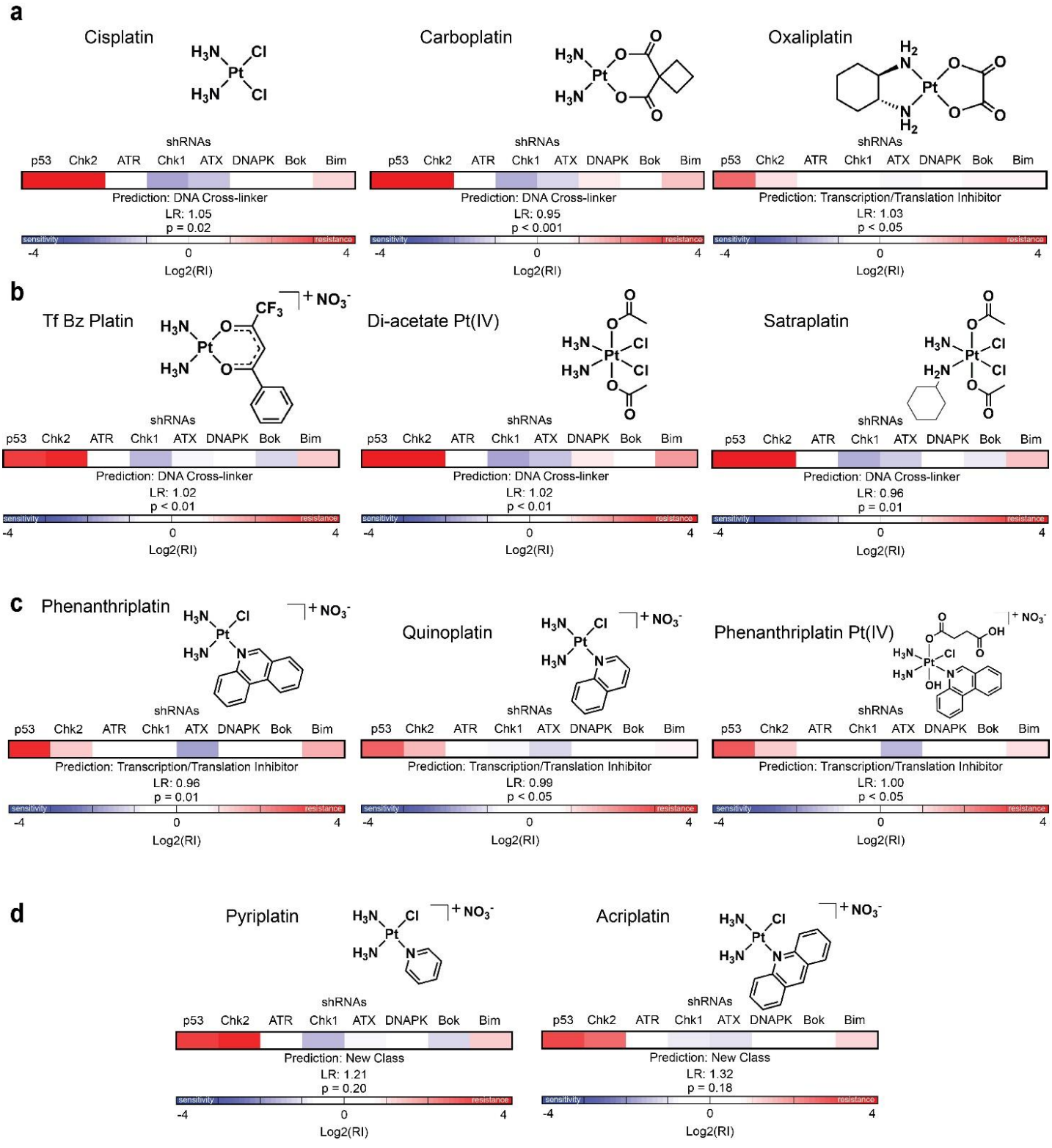

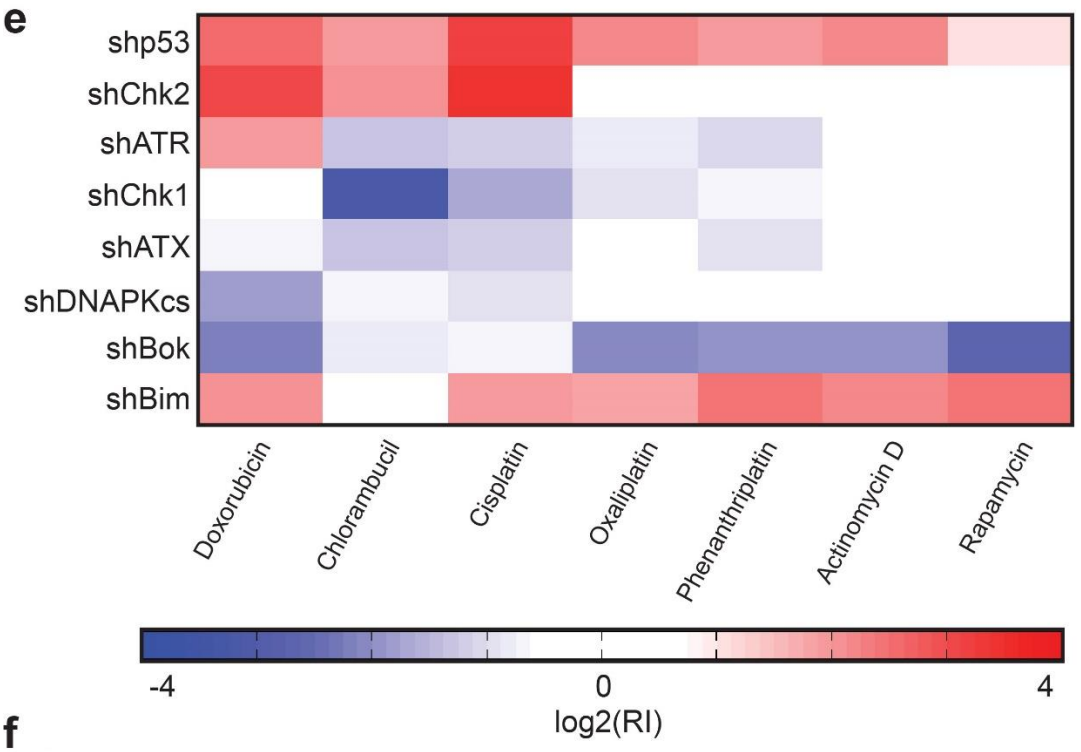

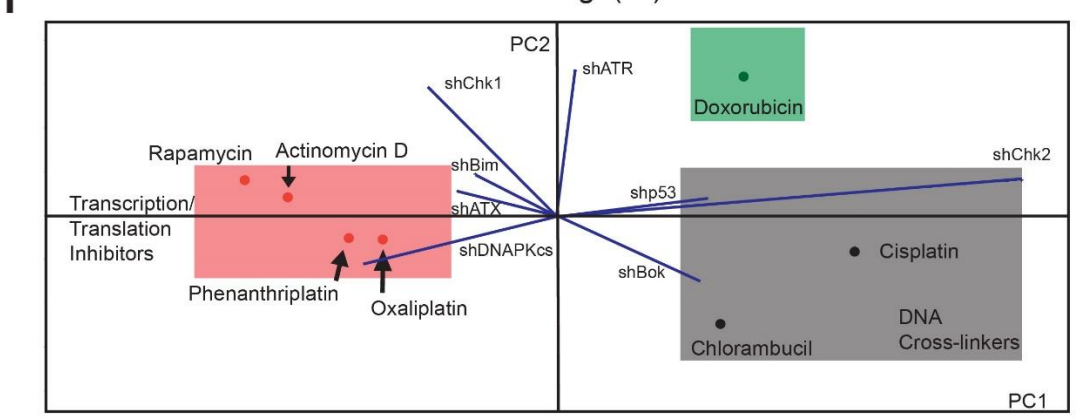

Principal Component	1	2
% Variance Explained	46.3	37.3

Principal Component 1 Loadings							
p53	Chk2	ATR	Chk1	ATX	DNAPKcs	Bok	Bim
0.26	0.81	0.03	-0.22	-0.17	-0.33	-0.24	-0.14

(**a**) Signatures and predictions in *Eμ-Myc p19*$^{Arf-/-}$ lymphoma cells of the three clinically approved platinum agents: cisplatin, carboplatin and oxaliplatin. (**b**) Additional compounds that classify as DNA cross-linkers in *Eμ-Myc p19*$^{Arf-/-}$ lymphoma cells. (**c**) Additional compounds that classify as transcription/translation inhibitors in *Eμ-Myc p19*$^{Arf-/-}$ lymphoma cells. (**d**) *Eμ-Myc p19*$^{Arf-/-}$ lymphoma cells tested with compounds that classify as a “New Class”, or compounds not represented in the reference set. (**e**) Heat map showing platinum compound signatures in murine p185+ *BCR-Abl* $^{p19arf-/-}$ cells with reference compounds, rapamycin, actinomycin D and chlorambucil included. (**f**) Principal component analysis of the p185+ *BCR-Abl* $^{p19arf-/-}$ signatures of platinum compounds. Tables show the percent variance explained by each principal component and the principal component 1 loadings depicting the percent contribution of each of the eight shRNAs for the PCA shown above.

Supplementary Figure S3. RNAi signatures of cisplatin, oxaliplatin and phenanthriplatin in combination with 5-fluorouracil preserve mechanism of action differences among the platinum agents.

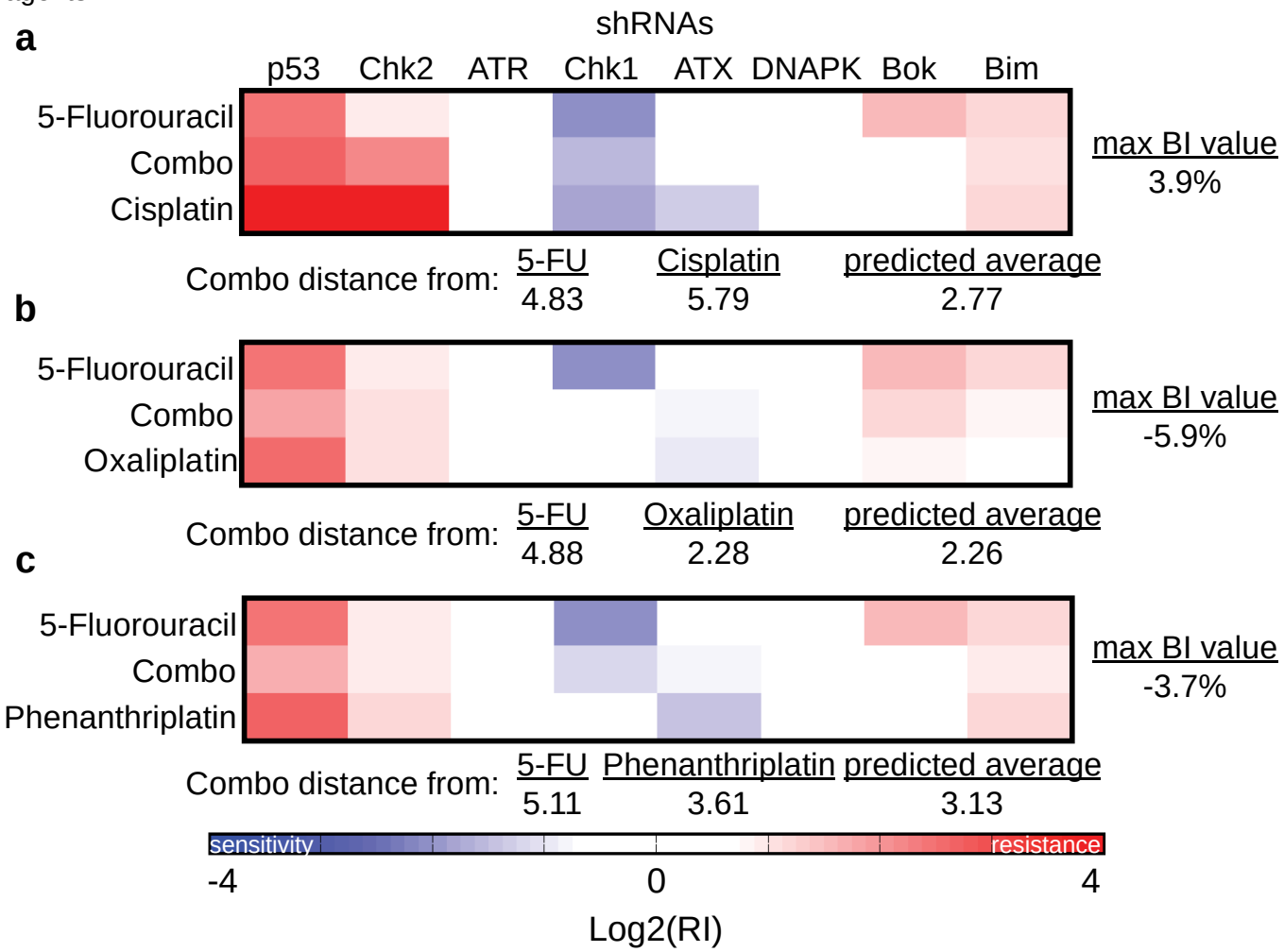

RNAi signatures of (**a**) cisplatin, (**b**) oxaliplatin and (**c**) phenanthriplatin alone and in combination with 5-fluorouracil in *Eμ-Myc p19*$^{Arf-/-}$ lymphoma cells. The combination differences represent the sum of absolute differences between the combination and the individual signatures or the combination signature predicted from a 1:1 average of the two individual signatures in question. Max BI value represents the maximum percent excess over Bliss Independence for the given combination.

Supplementary Figure S4. Platinum agent structure-based hierarchical clustering via Tanimoto coefficients.

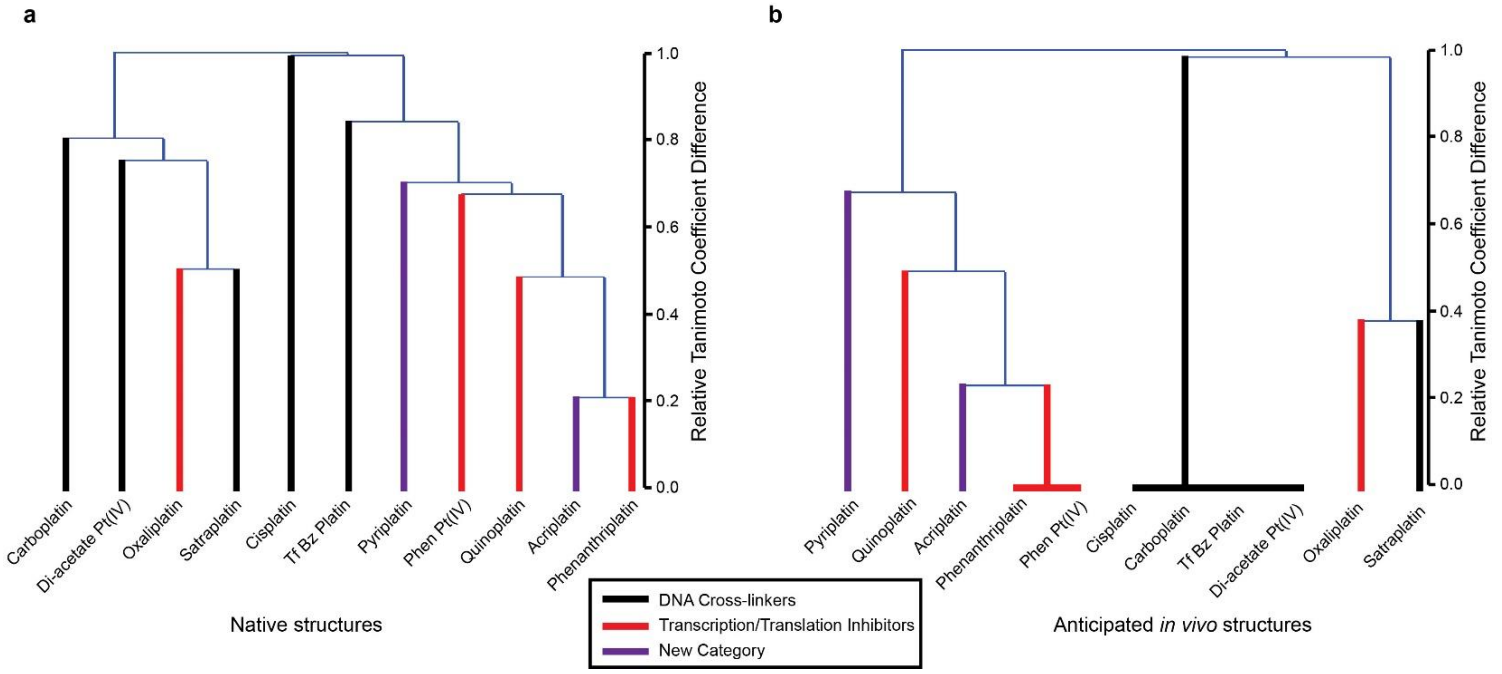

(**a**) Clustering by compound structure. (**b**) Clustering by structure as would be found at physiological conditions within the cell.

Supplementary Figure S5. DNA damage repair and tolerance hairpin responses, and knockdown validation.

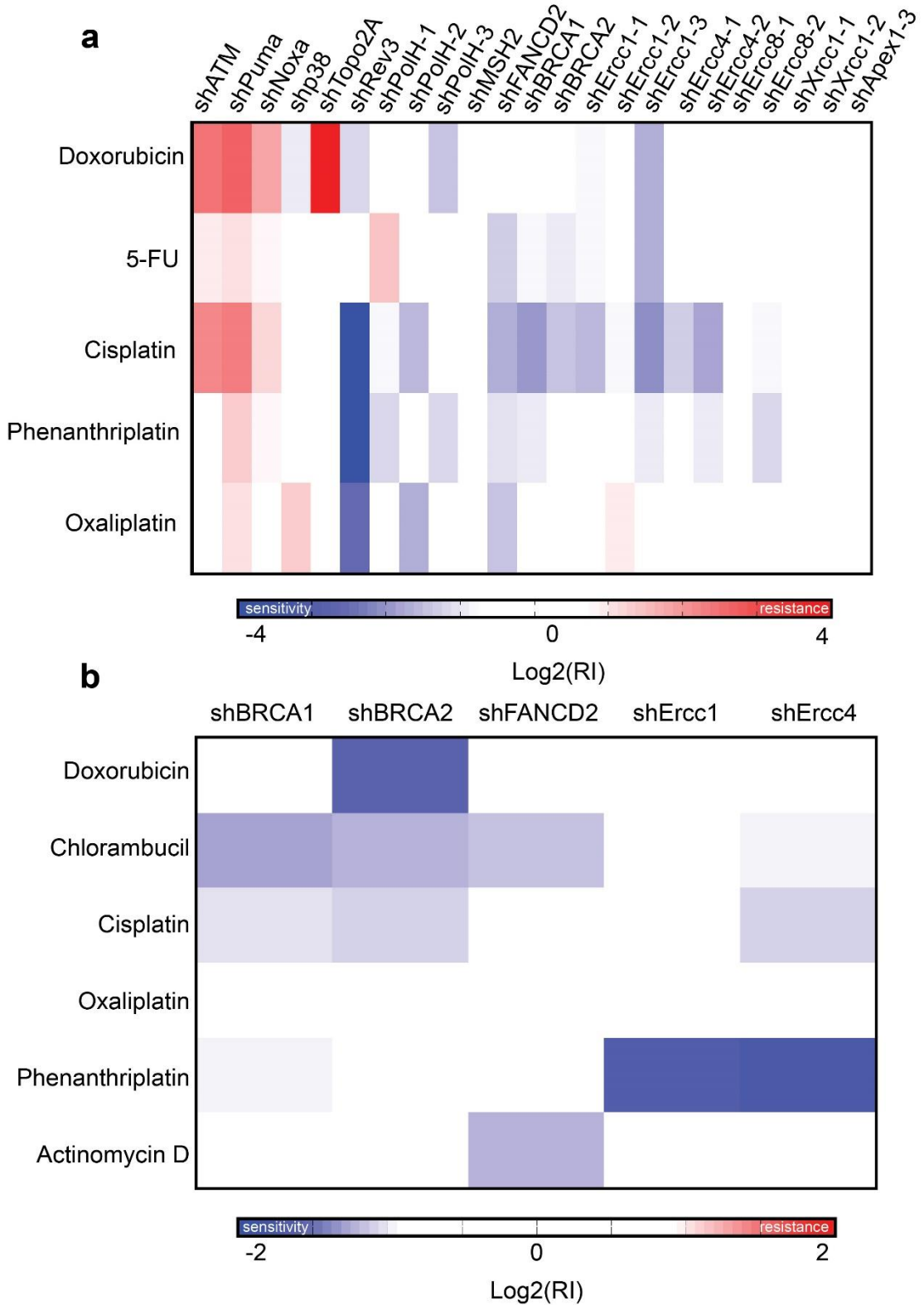

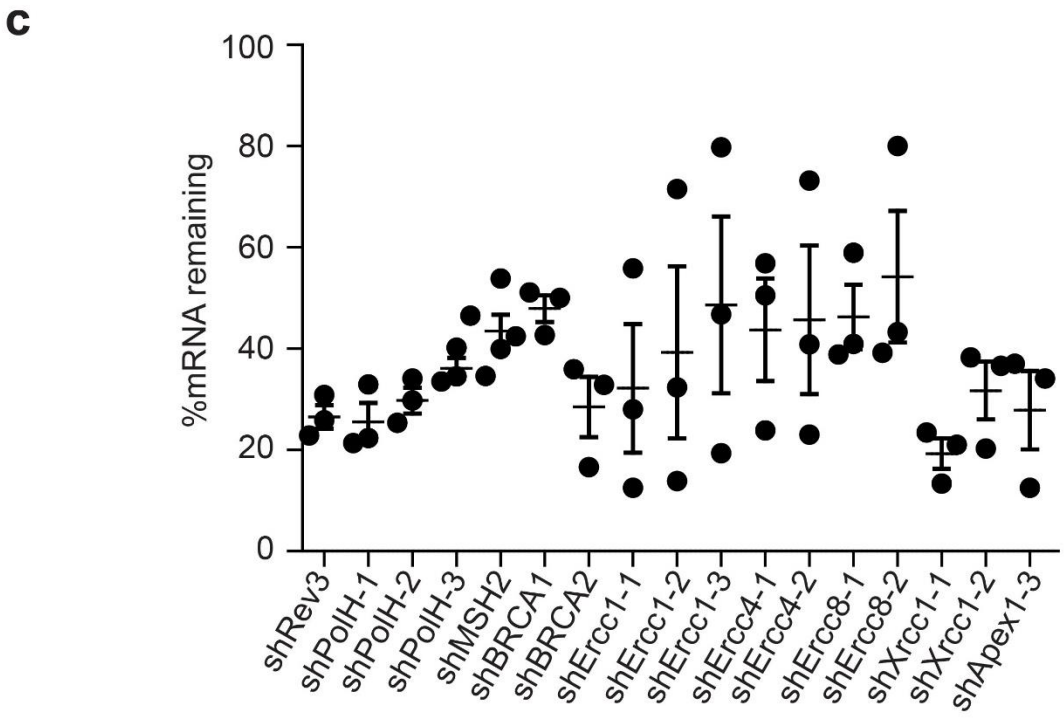

(**a**) Heatmap depicting sensitivity and resistance to drugs in *Eμ-Myc p19*$^{Arf-/-}$ lymphoma cells upon transduction of various hairpins. (**b**) Heatmap depicting sensitivity and resistance to drugs in *Eμ-Myc p53*$^{-/-}$ lymphoma cells upon transduction of various hairpins. Only the hairpins with the best knockdown were chosen for use here. (**c**) Results of qPCR for hairpin target knockdown in *Eμ-Myc p19*$^{Arf-/-}$ lymphoma cells (n=3 from two different thaws of cells and infections. qPCR technical replicates are averaged in each of the individual experiments). Data are represented as mean ± SEM.

Supplementary Figure S6. Cell cycle profiles resulting from treatment of *Eμ-Myc p19*$^{Arf-/-}$, A549 and LoVo cells by the indicated platinum anti-cancer agents.

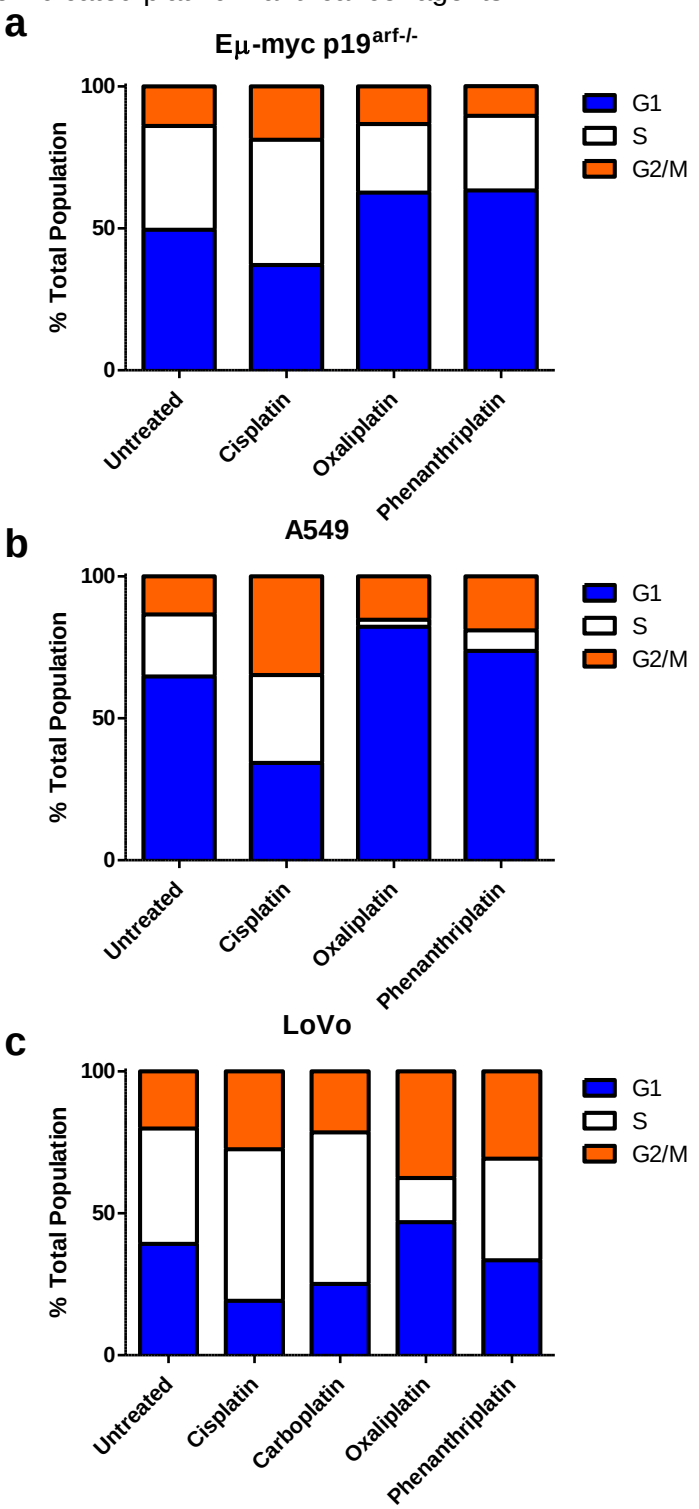

(**a**) Reproduced from **Fig. 3b**, cell cycle stage proportions resulting from 12 h of treatment with the indicated agents for *Eμ-Myc p19*$^{arf-/-}$ cells. (**b**) Cell cycle stage proportions resulting from 24 h of treatment with the indicated agents for A549 cells. (**c**) Cell cycle stage proportions resulting from 24 h of treatment with the indicated agents for LoVo cells.

Supplementary Figure S7. p21 is upregulated more quickly and its loss sensitizes to oxaliplatin and phenanthriplatin treatment.

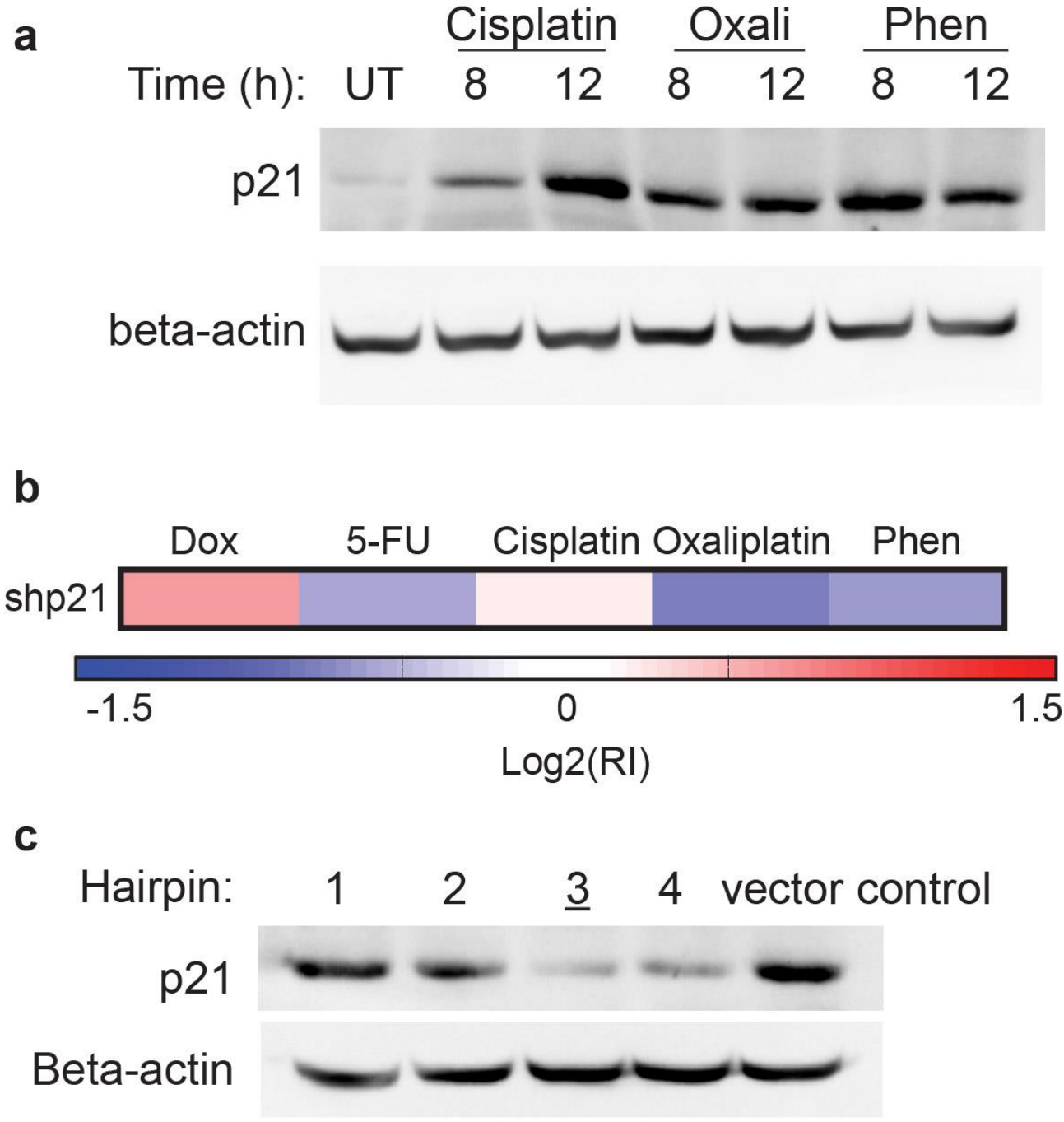

(**a**) Western blot for p21 after cisplatin, oxaliplatin or phenanthriplatin treatment at 8 h and 12 h *Eμ-Myc p19*$^{Arf-/-}$ lymphoma cells. (**b**) Heatmap depicting sensitivity and resistance to drugs in *Eμ-Myc p19*$^{Arf-/-}$ lymphoma cells upon transduction of a p21 hairpin. (**c**) Western blot showing knockdown of four hairpins against p21 and the vector control after 12 h of cisplatin treatment at the LD80-90 in *Eμ-Myc p19*$^{Arf-/-}$ lymphoma cells. Hairpin three, underlined, was the one used in the two figures above.

Supplementary Figure S8. Oxaliplatin and phenanthriplatin exhibit distinct differences from cisplatin in γ-H2AX and p53 signaling in *Eμ-Myc p19*$^{Arf-/-}$ lymphoma cells.

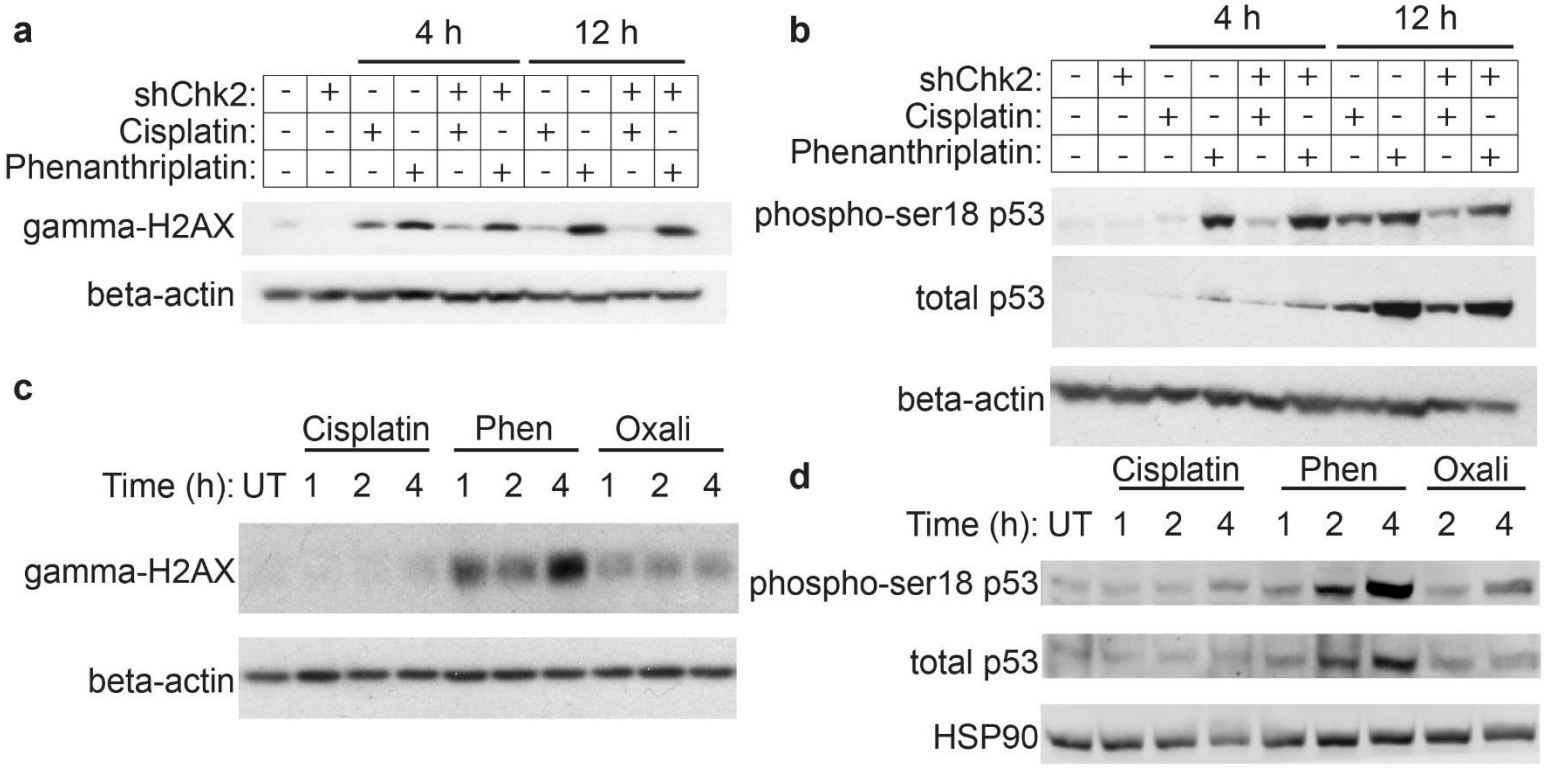

(**a**) Western blot for γ-H2AX after cisplatin or phenanthriplatin treatment with or without shChk2 or shChk1 at 4 h and 12 h. (**b**) Western blot for phospho-ser18 and total p53 after cisplatin or phenanthriplatin treatment with or without shChk2 or shChk1 at 4 h and 12 h. (**c**) Western blot for γ-H2AX after cisplatin, phenanthriplatin or oxaliplatin treatment at 1, 2 and 4 h. (**d**) Western blot for phospho-ser18 and total p53 after cisplatin, phenanthriplatin or oxaliplatin treatment at 1, 2 and 4 h.

Supplementary Figure S9. Kinetics of apoptosis of cisplatin, oxaliplatin, phenanthriplatin and reference drugs in *Eμ-Myc p19*$^{Arf-/-}$ lymphoma cells

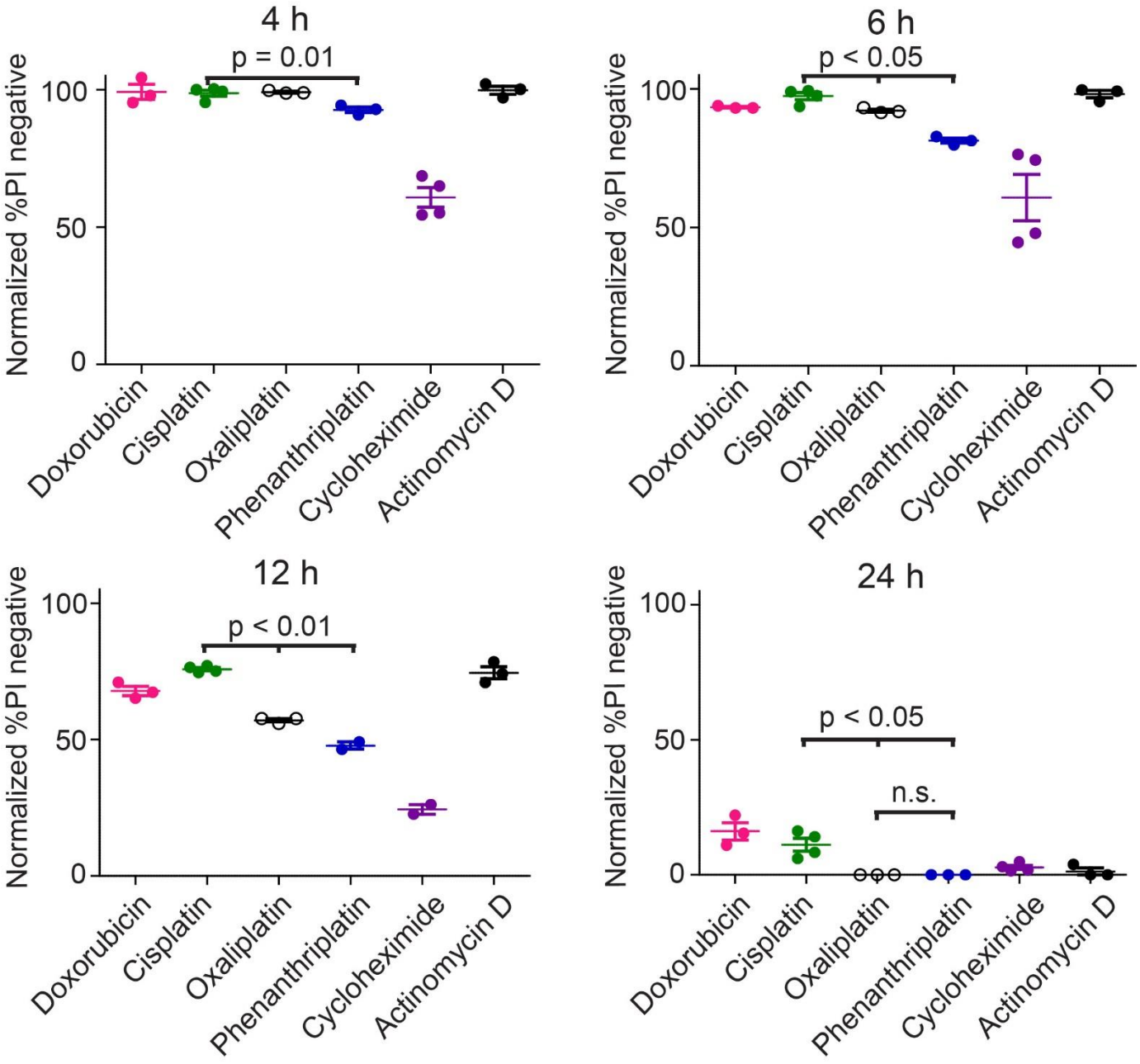

Actinomycin D is a representative transcription inhibitor. Doxorubicin is a DNA damage agent that works as a Top2 poison. Cycloheximide is a translation inhibitor. Percent of cells that were PI negative were measured at 4, 6, 12, 24 and 48 h after treatment by flow cytometry. Only doses that yielded an LD80-90 at 48 h were included in this analysis (n=4 for cisplatin and cycloheximide and n=3 for the other treatments). Data are represented as mean ± SEM and originate from three different doses on three independent cultures.

Supplementary Figure S10. DNA damage response pathway analysis in human cancer cell lines.

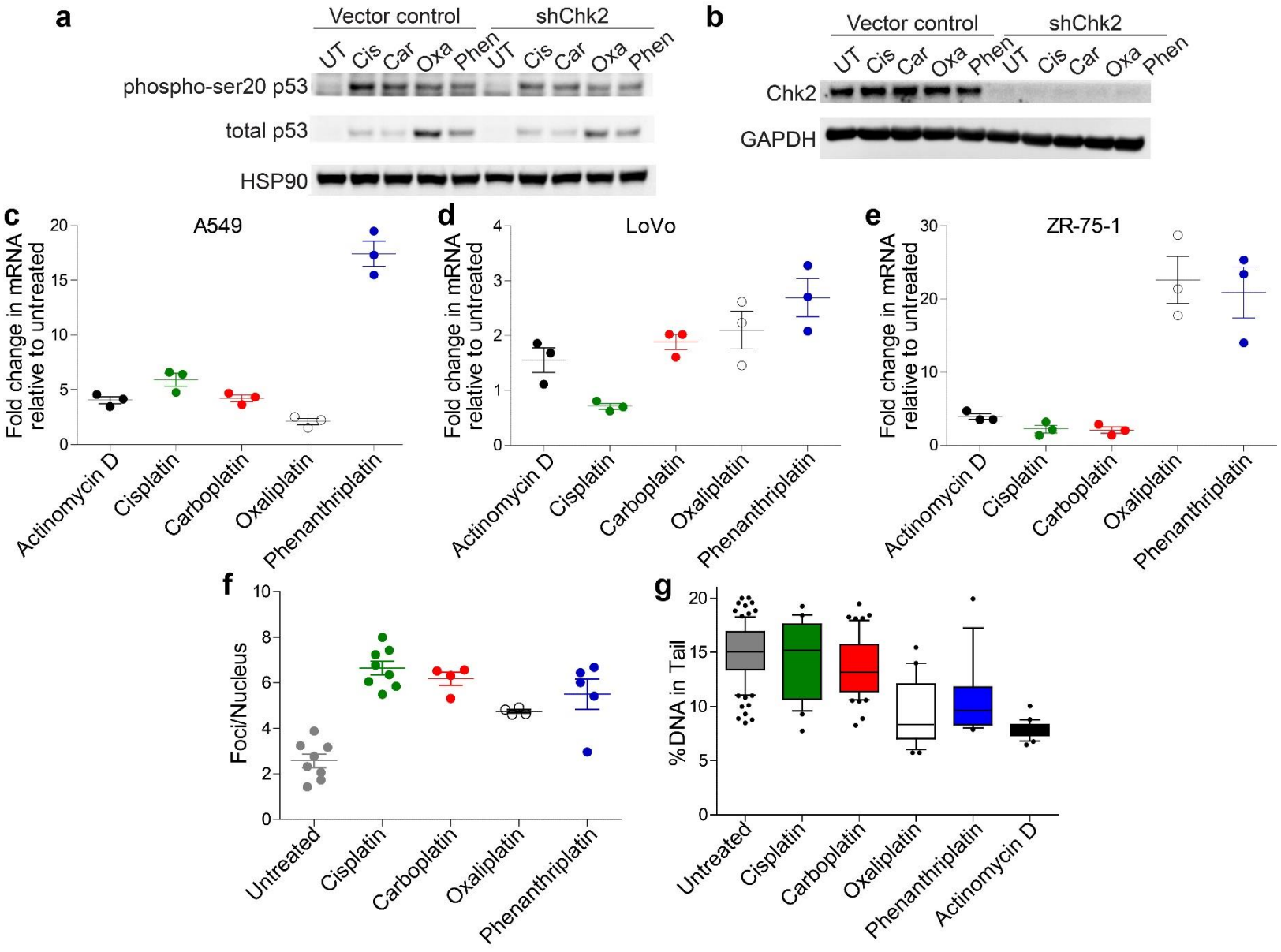

(**a**) Western blot for phospho-ser20 and total p53 after no treatment (UT), cisplatin (Cis), carboplatin (Car), oxaliplatin (Oxa) or phenanthriplatin (Phen) treatment with or without shChk2 at 24 h in LoVo cells. (**b**) Western blot for total Chk2 levels after no treatment (UT), cisplatin (Cis), carboplatin (Car), oxaliplatin (Oxa) or phenanthriplatin (Phen) treatment with or without shChk2 at 24 h in LoVo cells. Results of qPCR analysis conducted for Noxa after 12 h treatment with the indicated agents for (**d**) A549, (**e**) LoVo, (**f**) ZR-75-1 cells. Data are represented as mean ± SEM and result from three qPCR runs of two batches of cDNA made from the same RNA that resulted from one treatment of cells. (**g**) Foci per nucleus for each condition at 12 h after treatment of LoVo cells. Data are represented as mean ± SEM and derived from 8, 8, 4, 4 and 5 fields from untreated, cisplatin, carboplatin, oxaliplatin and phenanthriplatin conditions,

respectively. $p < 0.01$ (**) or $p < 0.001$ (***) for each group relative to untreated or cisplatin by one-way ANOVA with Dunnett's Multiple Comparison Test. (**h**) Quantification of percent DNA in tail via nE□tral comet assay 24 h after indicated drug treatment of ZR-75-1 cells. Data are represented as mean ± SEM and 94, 27, 52, 24, 14 and 21 comets were analyzed for the untreated, cisplatin, carboplatin, oxaliplatin, phenanthriplatin and actinomycin D conditions, respectively.. $p < 0.05$ (*) or $p < 0.001$ (***) for each group relative to untreated or cisplatin by one-way ANOVA with Dunnett's Multiple Comparison Test.

Supplementary Figure S11. RNA polymerase II transcribed mRNAs are unchanged in response to oxaliplatin and phenanthriplatin treatment in *Eμ-Myc p19*$^{Arf-/-}$ lymphoma cells.

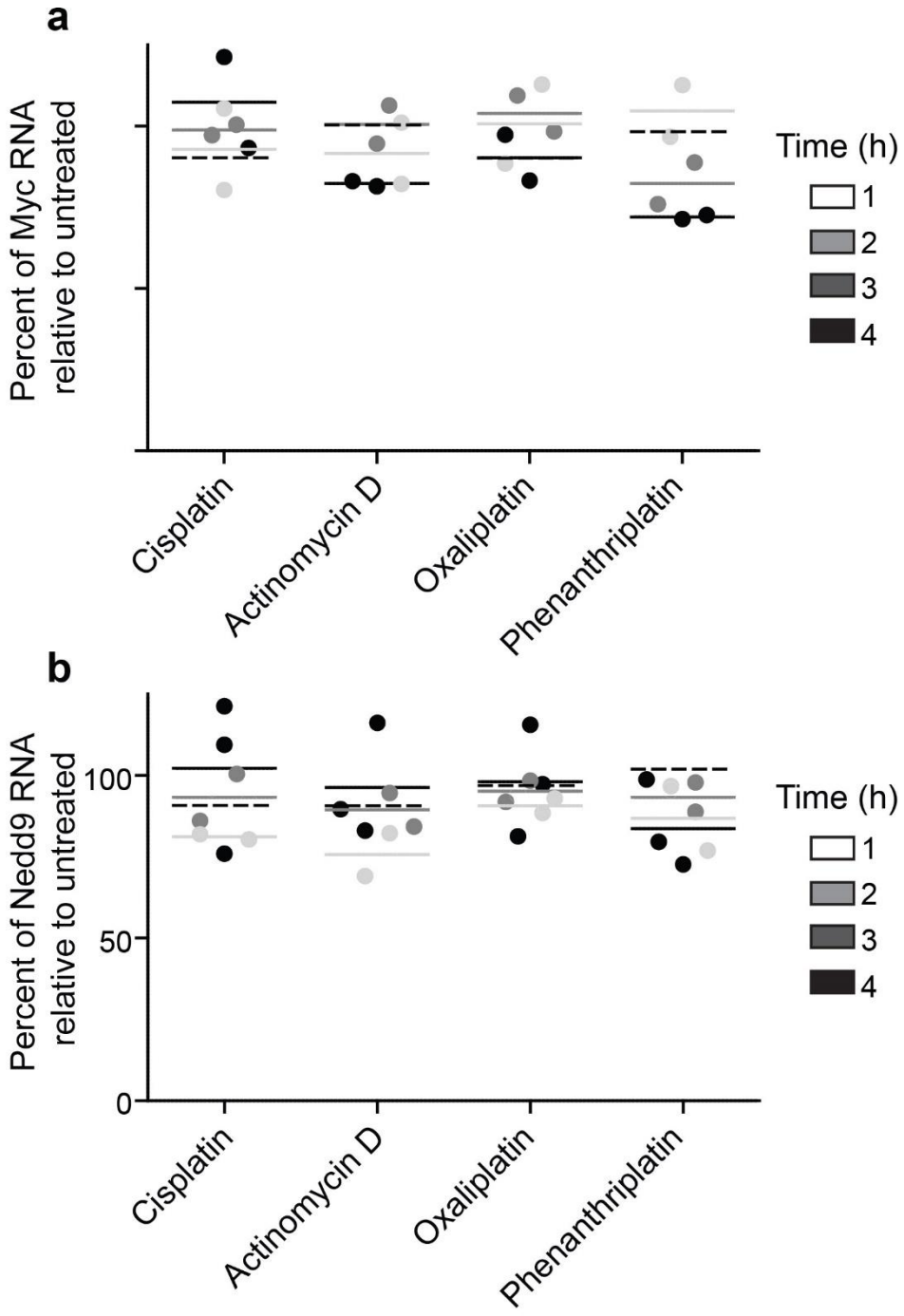

(**a**) Percent of Myc mRNA at various time points after treatment as determined by qPCR and normalized to GAPDH. Data are represented as mean ± SEM from 2 independent doses and cultures. (**b**) Percent of Nedd9 mRNA at various time points after treatment as determined by qPCR and normalized to GAPDH. Data are represented as mean ± SEM from 2 independent doses and cultures except 1 and 6 h which had three.

Supplementary Figure S12. Effects of RPL11 knockdown on platinum agent response and p53 signaling and shRPL11 knockdown validation.

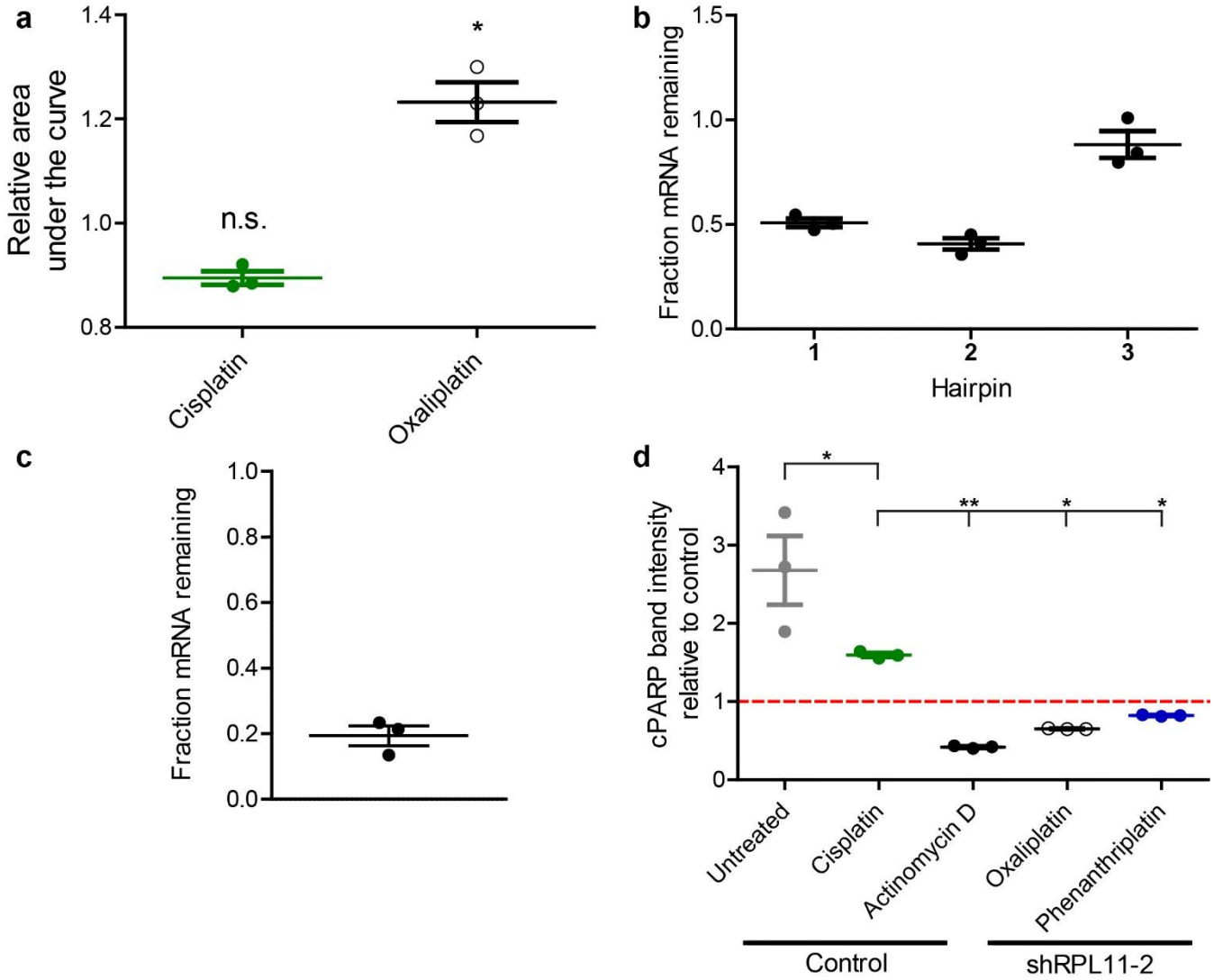

(**a**) A549 cells harboring either shRPL11 or vector control were exposed to dose ranges of the indicated platinum agents for 96 h. n=3 for cisplatin and oxaliplatin as technical replicates. Relative area under the curve between control and hairpin lines are reported. $p < 0.05$ (*) by Student's t-test. Data are represented as mean ± SEM. (**b**) Results of qPCR for RPL11 knockdown in *Eμ-Myc p19*$^{Arf-/-}$ lymphoma cells after 24 h of doxycycline exposure from two independent cultures and three qPCR runs. Data are represented as mean ± SEM. (**c**) Results of qPCR for RPL11 knockdown in human SW480 cells after 24 h of doxycycline exposure. n=3 qPCR runs from the same culture. Data are represented as mean ± SEM. (**d**) Values indicate an increase in cleaved PARP when RPL11 is knocked down whereas values below one indicate a decrease in cleaved PARP when RPL11 is knocked down. Quantification is a result of three separate densitometry analyses via ImageJ (n = 3). Data are represented as mean ± SEM. $p < 0.05$ (*), $p < 0.01$ (**) or $p < 0.001$ (***) for each group relative to untreated or cisplatin by one-way ANOVA with Dunnett's Multiple Comparison Test. Actinomycin D, oxaliplatin and phenanthriplatin have $p < 0.001$ relative to untreated.

Supplementary Figure S13. Immunofluorescence of nucleolar proteins indicates distinct mechanisms of action among platinum agents.

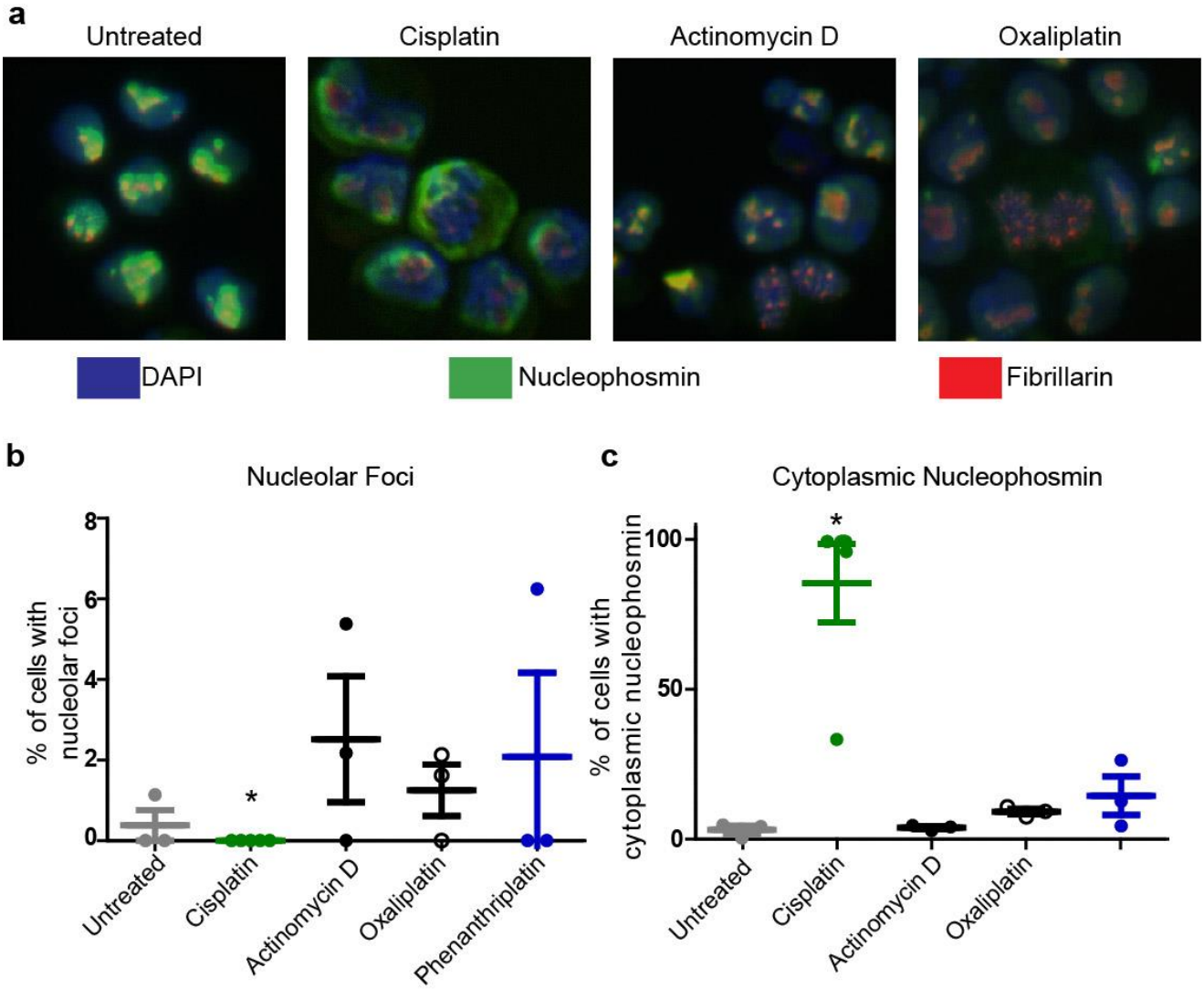

(**a**) Representative images at 40x magnification of nucleophosmin (green) and fibrillarin (red) immunofluorescence staining 8 h after treatment with the indicated compounds in of *Eμ-Myc p19*$^{Arf-/-}$ lymphoma cells. DAPI is in blue. (**b**) Quantification of the percent of cells possessing nucleolar foci 8 h after treatment. Data are represented as mean ± SEM. (*) represents the inability to perform a statistical significance test due to the lack of any nucleolar foci in that condition. (**c**) Quantification of the percent of cells possessing cytoplasmic nucleophosmin 8 h after treatment. Data are represented as mean ± SEM. $p < 0.0001$ (*) for each group relative to cisplatin by one-way ANOVA with Dunnett's Multiple Comparison Test. Three fields from one experiment were analyzed for each condition except for cisplatin for which 5 fields were analyzed.

Supplementary Figure S14. Polysome gradients resulting from treatment with platinum agents in *Eμ-Myc p19*$^{arf-/-}$cells.

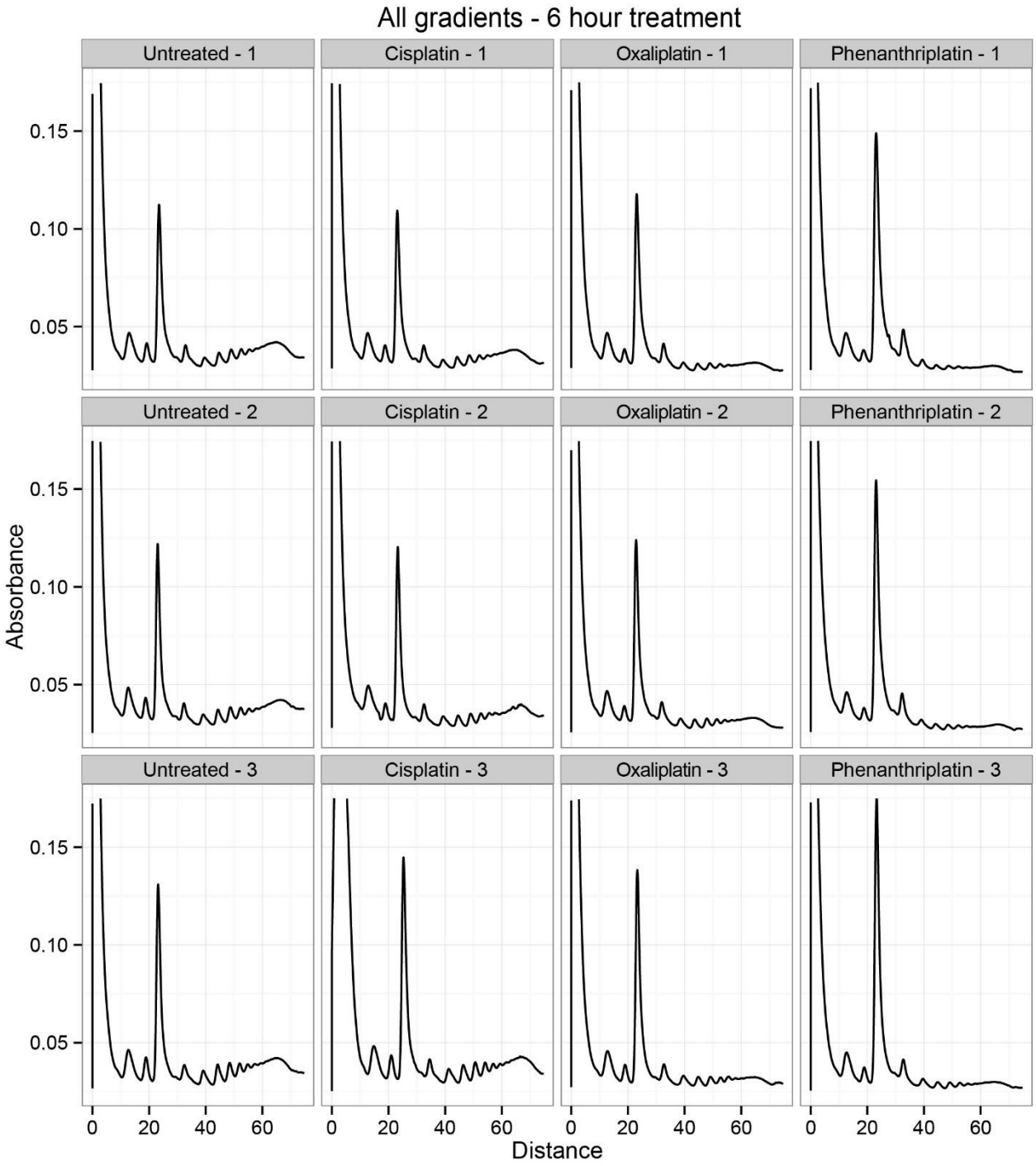

Supplementary Figure S15. Oxaliplatin disrupts protein synthesis as measured by O-propargyl-puromycin (OPP) incorporation.

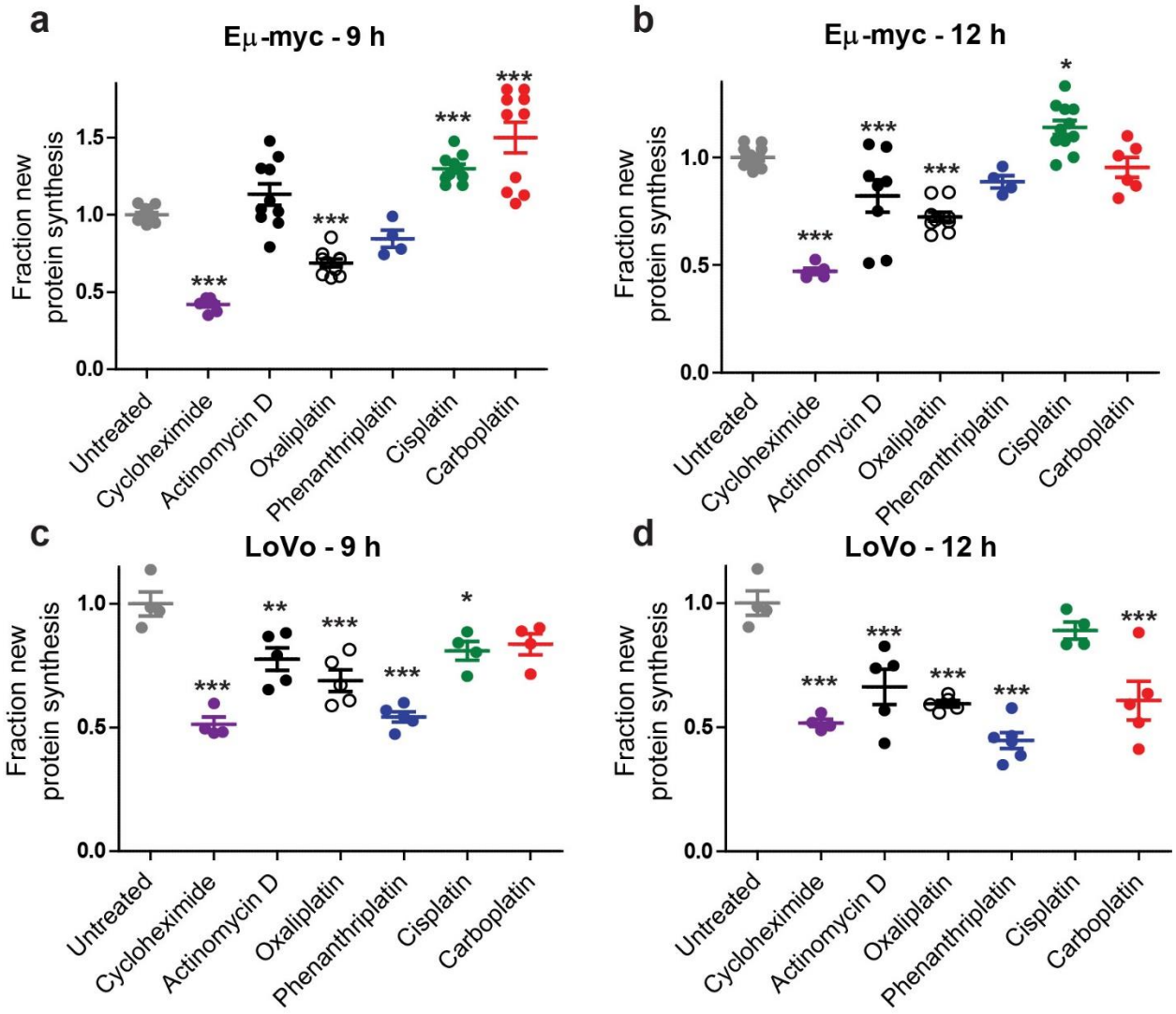

Fraction of newly synthesized protein relative to the untreated condition for (**a**) *Eμ-Myc p19$^{Arf-/-}$* lymphoma cells at 9 h (reproduced from **Fig. 5g**), (**b**) *Eμ-Myc p19$^{Arf-/-}$* lymphoma cells at 12h, (**c**) LoVo colorectal cancer cells at 9 h, and (**d**) LoVo colorectal cancer cells at 12 h. Data are represented as mean ± SEM. $p < 0.05$ (*), $p < 0.01$ (**) or $p < 0.001$ (***) for each group relative to untreated by one-way ANOVA with Dunnett's Multiple Comparison Test. For *Eμ-Myc p19$^{Arf-/-}$* lymphoma cells at 9 h, number of fields analyzed was 11 for untreated, 10 for actinomycin D, oxaliplatin, cisplatin and carboplatin, 7 for cycloheximide and 4 for phenanthriplatin. For *Eμ-Myc p19$^{Arf-/-}$* lymphoma cells at 12 h, number of fields analyzed was 11 for untreated and cisplatin, 10 for oxaliplatin, 8 for actinomycin D, 6 for carboplatin, 5 for cycloheximide and 4 for phenanthriplatin. For LoVo ells at 9 h, number of fields analyzed was 5 for actinomycin D, oxaliplatin, phenanthriplatin and 4 for the rest. For LoVo ells at 12 h, number of fields analyzed was 6 for phenanthriplatin, 5 for actinomycin D, oxaliplatin, phenanthriplatin and 4 for the rest. All conditions were dosed, fixed and analyzed on two different dates from the same batch of cells.

Supplementary Figure S16. Scatter plots of NCI-60 oxaliplatin cell line responses versus the top 4 genes that correlate to oxaliplatin response.

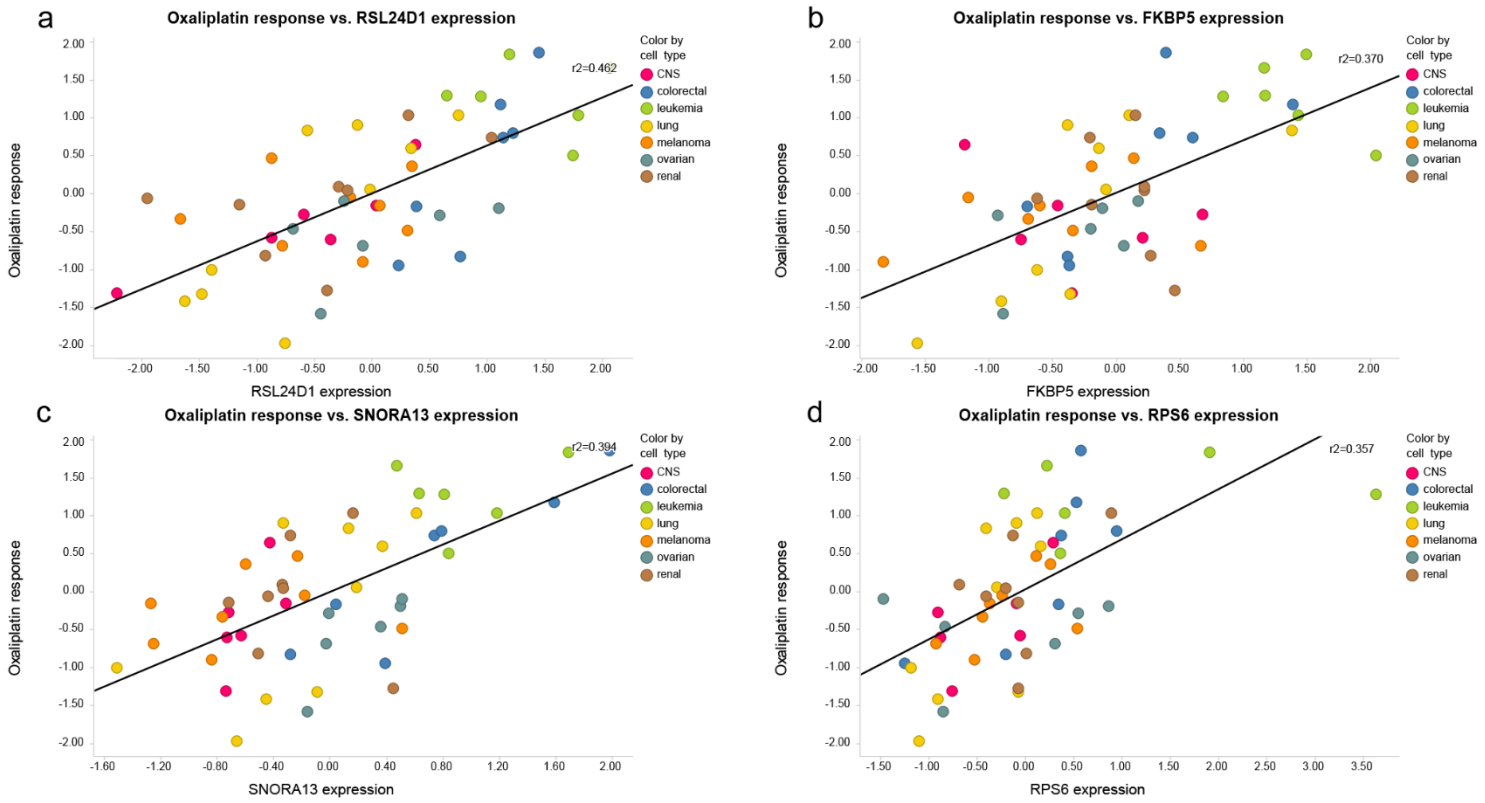

(**a**) Scatter plot comparing oxaliplatin drug response to RSL24D1 expression. (**b**) Scatter plot comparing oxaliplatin drug response to FKBP5 expression. (**c**) Scatter plot comparing oxaliplatin drug response to SNORA13 expression. (**d**) Scatter plot comparing oxaliplatin drug response to RPS6 expression.

Supplementary Figure S17. Validation of PTEN knockdown via qPCR in *Eμ-Myc p19*$^{Arf-/-}$ lymphoma cells.

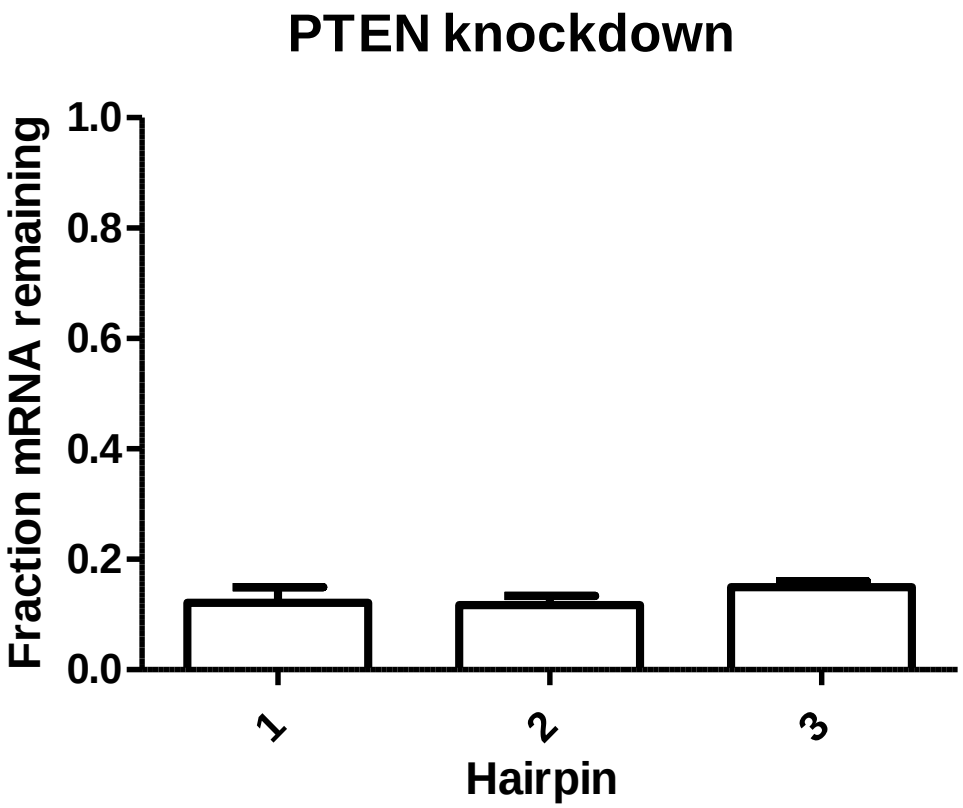

Results of qPCR for PTEN knockdown in *Eμ-Myc p19*$^{Arf-/-}$ lymphoma cells (n=3). Data are represented as mean ± SEM from three different qPCR experiments from one culture of cells.

Supplementary Figure S18. Scatter plots of TCGA cancer datasets for which there is a significant correlation of translation metagene expression with APC expression.

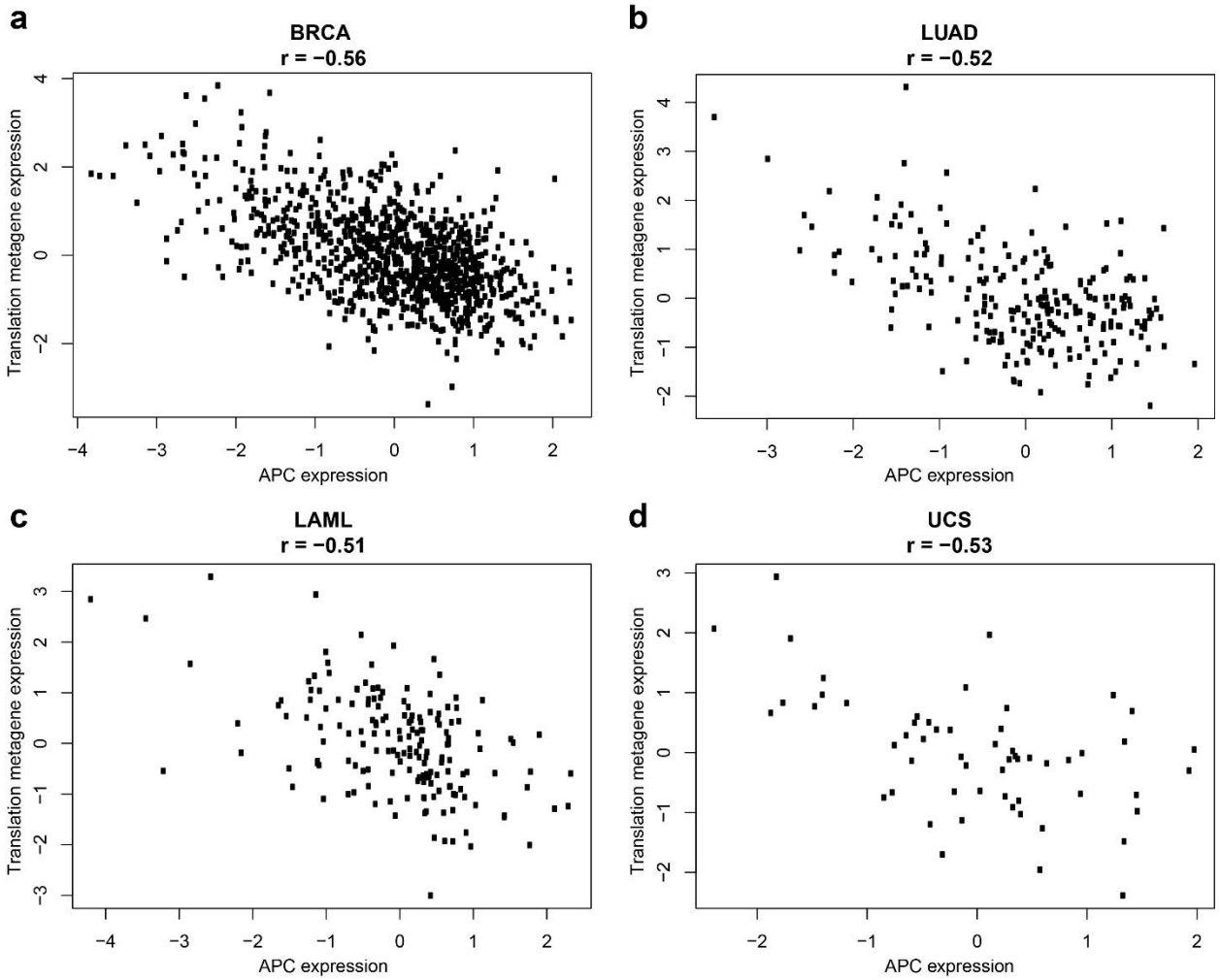

Scatter plots and correlation values of translation metagene expression (average expression values of 120 translation machinery genes) versus APC expression from the TCGA for (**a**) breast invasive carcinoma, (**b**) lung adenocarcinoma, (**c**) acute myeloid lE□kemia and (**d**) uterine carcinosarcoma.

Supplementary Figure S19. Full gels for all western blots.

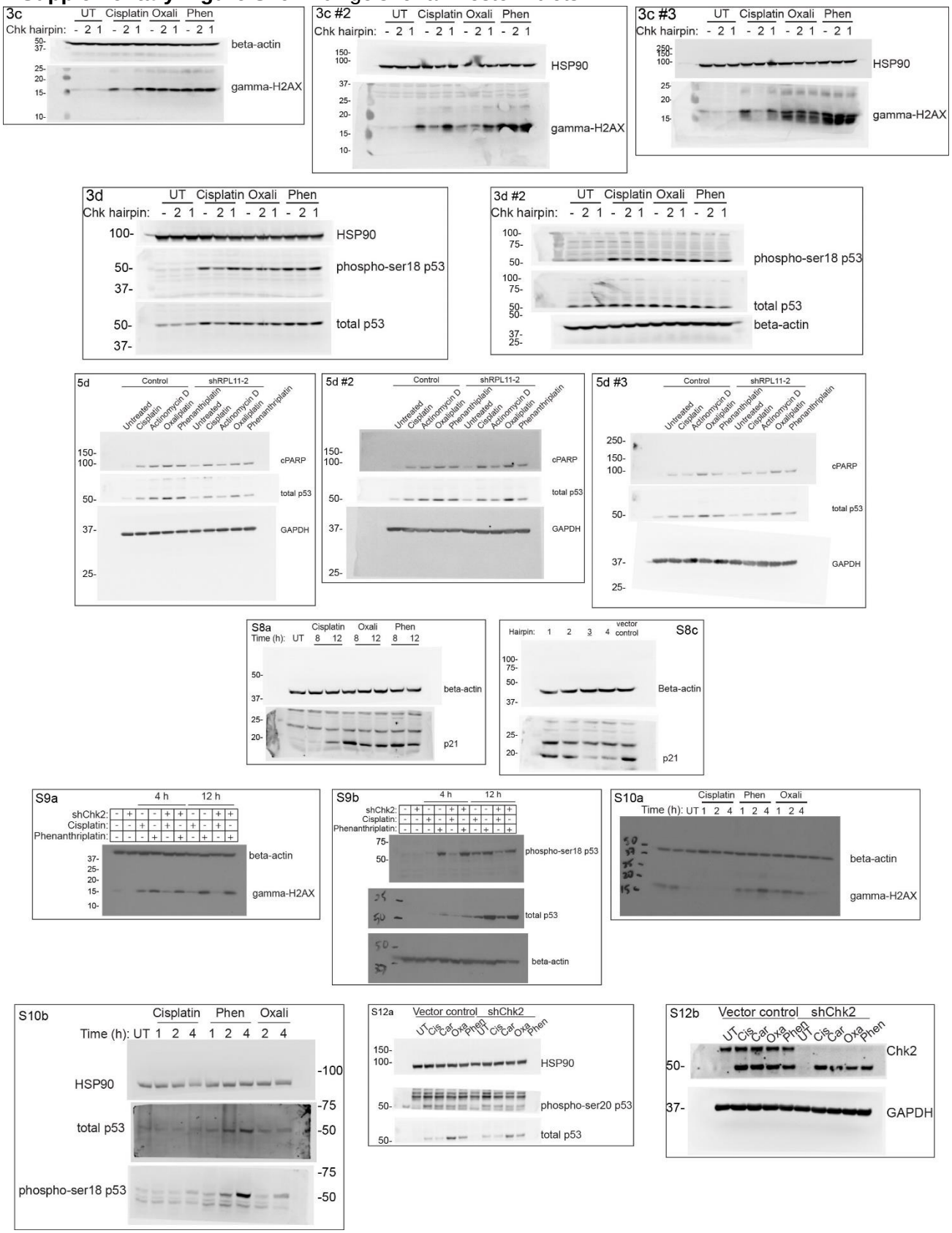

Supplementary Table S1. Reference set drugs and classes

Top2 Poisons	Doxorubicin
	Etoposide
	Daunorubicin
	Mitoxantrone
DNA cross-linkers	Maphosphomide
	Mitomycin C
	Chlorambucil
	Busulfan
	Carmustine
	Thiotepa
	Melphalan
Single-strand Break Inducers	Streptozocin
	6-Thioguanine
	Temozolomide
	Irinotecan
	Camptothecin
Nucleotide Depletion Agents	Hydroxyurea
	Gemcitabine
	Methothrexate
	5-Fluorouracil
Spindle Poisons	Vinblastine
	Noscapine
	Vincristine
	Taxol
	2-Methoxyestradiol
Transcription/Translation Inhibitors	Actinomycin D
	Rapamycin
	Roscovitine
	Puromycin
HDAC or DNMT Inhibitors	SAHA
	Decitabine
	Zebularine
	Scriptaid
HSP90 Inhibitors	17-AAG
	PU-H71-BR
	BIIB021
	VER-50589
	Neopentylamine-42

Supplementary Table S2. Data used to generate heat map of **Fig. 1d**.

	shp53	shChk2	shATR	shChk1	shATX	shDNAPKcs	shBok	shBim
Chlorambucil	4.031	4.344	-0.142	-1.920	-0.594	0.598	-1.263	1.427
Cisplatin	4.228	4.339	-0.077	-1.795	-1.393	0.660	-0.399	1.228
Carboplatin	4.417	4.667	0.293	-1.684	-1.218	0.913	-0.597	1.481
Satraplatin	4.488	4.203	0.069	-1.660	-1.264	0.542	-0.960	1.462
Tf Bz Platin	4.040	4.368	0.098	-1.748	-1.287	0.661	-0.585	1.274
Di-acetate Pt(IV)	4.850	4.905	0.475	-1.773	-1.420	0.927	-0.406	1.935
Pyriplatin	3.137	3.604	-0.172	-1.585	-0.806	0.575	-1.156	1.374
Acriplatin	3.116	2.571	0.286	-0.967	-1.125	0.447	-0.411	1.181
Quinoplatin	2.600	1.378	0.031	-0.642	-1.234	0.372	0.394	0.711
Phen Pt (IV)	2.748	1.454	0.020	-0.626	-1.429	0.547	0.449	1.034
Phenanthriplatin	2.679	1.239	0.022	-0.545	-1.426	0.344	0.324	1.171
Oxaliplatin	2.532	1.166	0.075	0.047	-0.963	0.041	0.881	0.725
Actinomycin D	3.023	0.071	0.959	-0.251	-1.611	0.111	-0.167	0.693
Rapamycin	1.990	-0.137	0.272	-0.942	-1.622	-0.042	0.873	0.901

Supplementary Table S3. Training set drug leave-one-out cross-validation of platinum agent signature classifications.

Compound	% same category as full training set	% p > 0.05
Cisplatin	100	100
Carboplatin	100	100
Oxaliplatin	100	100
Tf Bz Platin	100	100
Di-Acetate Pt(IV)	100	100
Satraplatin	100	100
Quinoplatin	100	100
Phenanthriplatin Pt(IV)	100	100
Pyriplatin	100	0*
Acriplatin	100	0*

*Drugs classifying as “new category”, by definition, have a p-value of greater than 0.05

Supplementary Table S4. Data used to generate PCA plot of **Fig. 1e**.

	shp53	shChk2	shATR	shChk1	shATX	shDNAPKcs	shBok	shBim
Chlorambucil	4.031	4.344	-0.142	-1.920	-0.594	0.598	-1.263	1.427
Cisplatin	4.251	4.354	-0.108	-1.831	-1.421	0.671	-0.420	1.249
Carboplatin	4.417	4.667	0.293	-1.684	-1.218	0.913	-0.597	1.481
Tf Bz Platin	4.040	4.368	0.097	-1.748	-1.287	0.661	-0.585	1.273
Pyriplatin	3.137	3.604	-0.172	-1.585	-0.806	0.575	-1.156	1.374
Acriplatin	3.115	2.571	0.286	-0.967	-1.125	0.447	-0.411	1.180
Quinoplatin	2.600	1.378	0.031	-0.642	-1.234	0.372	0.394	0.711
Phenanthriplatin	2.656	1.226	0.001	-0.529	-1.413	0.371	0.343	1.208
Oxaliplatin	2.527	1.138	0.151	0.019	-0.906	0.095	0.902	0.732
Roscovitine	3.589	-0.114	0.812	-0.137	-0.926	0.212	0.071	1.672
Puromycin	2.420	0.903	0.261	-1.206	-2.008	0.161	-0.516	0.619
Actinomycin D	3.023	0.071	0.959	-0.251	-1.611	0.111	-0.167	0.693
Rapamycin	1.990	-0.137	0.272	-0.942	-1.622	-0.042	0.873	0.901
Doxorubicin	3.417	3.107	1.421	-0.376	-2.085	-1.419	-0.815	1.306
Etoposide	2.655	3.030	1.521	-0.168	-2.131	-0.277	-0.300	1.644
Daunorubicin	3.401	2.651	1.749	-0.218	-2.252	-0.690	-0.269	0.678
Mitomycin C	4.410	4.691	0.745	-1.669	-0.973	0.938	-0.987	1.421
Di-acetate Pt(IV)	4.850	4.905	0.475	-1.772	-1.420	0.927	-0.406	1.935
Phen Pt (IV)	2.748	1.454	0.020	-0.626	-1.429	0.547	0.449	1.033

Supplementary Table S5. DT40 isogenic mutant cell lines used in this study

Cell line	Major function of deleted (mutated) genes	Reference
KU70	NHEJ	1
LIGASE IV	NHEJ	2
DNA-PKcs	NHEJ	3
RAP80	NHEJ	4
ATM	Check point control	5
RAD9	Check point control	6
RAD17	Check point control	6
RAD52	HR	7
RAD54	HR	8
NBS1p70	HR	9,10
XRCC2	HR	11
XRCC3	HR	11
BRCA2 (truncated)	HR	12
RAD18	E3 ligase of PCNA, PRR	13
PCNAK164R	Ubiquitilation site of PCNA, PRR	14
PARP1	DNA damage sensing, poly(ADP-ribosyl)ation, SSB and DSB repair	15
TDP1	Removal of Top1 cleavage complex	16
TDP2	Removal of Top2 cleavage complex	17
TDP1/TDP2	(see above)	18
CtIP+/-/-	HR	19
CtIPs/-/-	HR, Removal of Top1 and Top2 cleavage complex	19
TDP1/CtIPs/-/-	(see above)	16
FANCC	Intercross-link repair, HR	20
FANCD2	Intercross-link repair, HR	21
FANCG	Intercross-link repair, HR	22
USP1	Intercross-link repair, HR	23
UAF1	Intercross-link repair, HR	23
SNM1A/SNM1B	Intercross-link repair	24
POLB	Base excision repair	25
POLL	Base excision repair	25
POLL/POLB	(see above)	25
POLN	TLS	26
POLQ	TLS	26
POLH	TLS	27
POLZ	TLS	28
POLH/POLZ	(see above)	29
FEN1	5’ flap endonuclease, base excision repair	30
XPA	Nuclear excision repair	31
XPG	Nuclear excision repair	32
FBH1	DNA helicase	33
BLM	RecQ helicase responsible for Bloom syndrome	34

*Knock-in mutant introduced K164R mutation into endogenous PCNA gene locus
NHEJ: nonhomologous end joining, HR: homologous recombination, PRR: post replication repair, TLS: translesion synthesis, Top1: topoisomerase I, Top2: topoiromserase II, SSB: single-strand break, DSB: double-strand break

1. Takata, M. *et al.* Homologous recombination and non-homologous end-joining pathways of DNA double-strand break repair have overlapping roles in the maintenance of chromosomal integrity in vertebrate cells. *EMBO J.* **17,** 5497–508 (1998).

2. Adachi, N., Ishino, T., Ishii, Y., Takeda, S. & Koyama, H. DNA ligase IV-deficient cells are more resistant to ionizing radiation in the absence of Ku70: Implications for DNA double-strand break repair. *Proc. Natl. Acad. Sci. U. S. A.* **98,** 12109–13 (2001).

3. Fukushima, T. *et al.* Genetic analysis of the DNA-dependent protein kinase reveals an inhibitory role of Ku in late S-G2 phase DNA double-strand break repair. *J. Biol. Chem.* **276,** 44413–8 (2001).

4. Iijima, J., Zeng, Z., Takeda, S. & Taniguchi, Y. RAP80 acts independently of BRCA1 in repair of topoisomerase II poison-induced DNA damage. *Cancer Res.* **70,** 8467–74 (2010).

5. Takao, N. *et al.* Disruption of ATM in p53-null cells causes multiple functional abnormalities in cellular response to ionizing radiation. *Oncogene* **18,** 7002–9 (1999).

6. Saberi, A. *et al.* The 9-1-1 DNA clamp is required for immunoglobulin gene conversion. *Mol. Cell. Biol.* **28,** 6113–22 (2008).

7. Yamaguchi-Iwai, Y. *et al.* Homologous recombination, but not DNA repair, is reduced in vertebrate cells deficient in RAD52. *Mol. Cell. Biol.* **18,** 6430–5 (1998).

8. Bezzubova, O., Silbergleit, A., Yamaguchi-Iwai, Y., Takeda, S. & Buerstedde, J. M. Reduced X-ray resistance and homologous recombination frequencies in a RAD54-/- mutant of the chicken DT40 cell line. *Cell* **89,** 185–93 (1997).

9. Nakahara, M. *et al.* Genetic evidence for single-strand lesions initiating Nbs1-dependent homologous recombination in diversification of Ig v in chicken B lymphocytes. *PLoS Genet.* **5,** e1000356 (2009).

10. Tauchi, H. *et al.* Nbs1 is essential for DNA repair by homologous recombination in higher vertebrate cells. *Nature* **420,** 93–8 (2002).

11. Takata, M. *et al.* Chromosome instability and defective recombinational repair in knockout mutants of the five Rad51 paralogs. *Mol. Cell. Biol.* **21,** 2858–66 (2001).

12. Hatanaka, A. *et al.* Similar effects of Brca2 truncation and Rad51 paralog deficiency on immunoglobulin V gene diversification in DT40 cells support an early role for Rad51 paralogs in homologous recombination. *Mol. Cell. Biol.* **25,** 1124–34 (2005).

13. Yamashita, Y. M. *et al.* RAD18 and RAD54 cooperatively contribute to maintenance of genomic stability in vertebrate cells. *EMBO J.* **21,** 5558–66 (2002).

14. Arakawa, H. *et al.* A role for PCNA ubiquitination in immunoglobulin hypermutation. *PLoS Biol.* **4,** e366 (2006).

15. Hochegger, H. *et al.* Parp-1 protects homologous recombination from interference by Ku and Ligase IV in vertebrate cells. *EMBO J.* **25,** 1305–14 (2006).

16. Murai, J. *et al.* Tyrosyl-DNA phosphodiesterase 1 (TDP1) repairs DNA damage induced by topoisomerases I and II and base alkylation in vertebrate cells. *J. Biol. Chem.* **287,** 12848–57 (2012).

17. Zeng, Z., Cortés-Ledesma, F., El Khamisy, S. F. & Caldecott, K. W. TDP2/TTRAP is the major 5'-tyrosyl DNA phosphodiesterase activity in vertebrate cells and is critical for

cellular resistance to topoisomerase II-induced DNA damage. *J. Biol. Chem.* **286,** 403–9 (2011).

18. Zeng, Z. *et al.* TDP2 promotes repair of topoisomerase I-mediated DNA damage in the absence of TDP1. *Nucleic Acids Res.* **40,** 8371–80 (2012).

19. Nakamura, K. *et al.* Collaborative action of Brca1 and CtIP in elimination of covalent modifications from double-strand breaks to facilitate subsequent break repair. *PLoS Genet.* **6,** e1000828 (2010).

20. Hirano, S. *et al.* Functional relationships of FANCC to homologous recombination, translesion synthesis, and BLM. *EMBO J.* **24,** 418–27 (2005).

21. Yamamoto, K. *et al.* Fanconi anemia protein FANCD2 promotes immunoglobulin gene conversion and DNA repair through a mechanism related to homologous recombination. *Mol. Cell. Biol.* **25,** 34–43 (2005).

22. Yamamoto, K. *et al.* Fanconi anemia FANCG protein in mitigating radiation- and enzyme-induced DNA double-strand breaks by homologous recombination in vertebrate cells. *Mol. Cell. Biol.* **23,** 5421–30 (2003).

23. Murai, J. *et al.* The USP1/UAF1 complex promotes double-strand break repair through homologous recombination. *Mol. Cell. Biol.* **31,** 2462–9 (2011).

24. Ishiai, M. *et al.* DNA cross-link repair protein SNM1A interacts with PIAS1 in nuclear focus formation. *Mol. Cell. Biol.* **24,** 10733–41 (2004).

25. Tano, K. *et al.* Interplay between DNA polymerases beta and lambda in repair of oxidation DNA damage in chicken DT40 cells. *DNA Repair (Amst).* **6,** 869–75 (2007).

26. Yoshimura, M. *et al.* Vertebrate POLQ and POLbeta cooperate in base excision repair of oxidative DNA damage. *Mol. Cell* **24,** 115–25 (2006).

27. Kawamoto, T. *et al.* Dual roles for DNA polymerase eta in homologous DNA recombination and translesion DNA synthesis. *Mol. Cell* **20,** 793–9 (2005).

28. Sonoda, E. *et al.* Multiple roles of Rev3, the catalytic subunit of polzeta in maintaining genome stability in vertebrates. *EMBO J.* **22,** 3188–97 (2003).

29. Hirota, K. *et al.* Simultaneous disruption of two DNA polymerases, Polη and Polζ, in Avian DT40 cells unmasks the role of Polη in cellular response to various DNA lesions. *PLoS Genet.* **6,** (2010).

30. Matsuzaki, Y., Adachi, N. & Koyama, H. Vertebrate cells lacking FEN-1 endonuclease are viable but hypersensitive to methylating agents and H2O2. *Nucleic Acids Res.* **30,** 3273–7 (2002).

31. Okada, T. *et al.* Involvement of vertebrate polkappa in Rad18-independent postreplication repair of UV damage. *J. Biol. Chem.* **277,** 48690–5 (2002).

32. Kikuchi, K. *et al.* Fen-1 facilitates homologous recombination by removing divergent sequences at DNA break ends. *Mol. Cell. Biol.* **25,** 6948–55 (2005).

33. Kohzaki, M. *et al.* Cooperative roles of vertebrate Fbh1 and Blm DNA helicases in avoidance of crossovers during recombination initiated by replication fork collapse. *Mol. Cell. Biol.* **27,** 2812–20 (2007).

34. Imamura, O. *et al.* Bloom helicase is involved in DNA surveillance in early S phase in vertebrate cells. *Oncogene* **20,** 1143–51 (2001).

Supplementary Table S6. Pairwise distances among homologous recombination and inter-strand cross-link repair genes of DT40 mutants treated with the indicated agents.

	Cisplatin	Carboplatin	Tf Bz Pt	Oxaliplatin	Phenanthriplatin
Cisplatin	0	1.03	1.54	3.36	5.16
Carboplatin		0	2.06	3.44	5.09
Tf Bz Platin			0	3.94	5.53
Oxaliplatin				0	2.40
Phenanthriplatin					0

Supplementary Table S7. Significant GSEA pathways upregulated in colorectal cancer relative to ovarian cancer.

NAME	Size	ES	NES	FDR q-value
KEGG STARCH AND SUCROSE METABOLISM	21	-0.63	-2.71	0.000
KEGG PENTOSE AND GLUCURONATE INTERCONVERSIONS	15	-0.71	-2.69	0.000
KEGG DRUG METABOLISM OTHER ENZYMES	23	-0.59	-2.68	0.000
KEGG RIBOSOME	16	-0.69	-2.64	0.000
KEGG RETINOL METABOLISM	31	-0.53	-2.57	0.000
KEGG METABOLISM OF XENOBIOTICS BY CYTOCHROME P450	32	-0.52	-2.53	0.000
KEGG DRUG METABOLISM CYTOCHROME P450	34	-0.50	-2.46	0.000
KEGG STEROID HORMONE BIOSYNTHESIS	27	-0.51	-2.33	0.000
KEGG CHEMOKINE SIGNALING PATHWAY	23	-0.43	-1.92	0.011

Supplementary Table S8. Top five GSEA pathways upregulated in ovarian cancer relative to colorectal cancer

NAME	Size	ES	NES	FDR q-value
LE□KOCYTE TRANSENDOTHELIAL MIGRATION	16	0.37	1.54	0.670
TIGHT JUNCTION	18	0.35	1.53	0.366
CELL ADHESION MOLECULES CAMS	24	0.33	1.52	0.254
PATHWAYS IN CANCER	37	0.27	1.42	0.210
AXON GUIDANCE	20	0.32	1.29	0.259

Supplementary Table S9: shRNA sequences used in this study.

Gene	mRNA Target Sequence
MSH2	CAGGATGCCATTGTTAAAGAA
PolH-1	CAGCTGGAATCTCACACAATA
PolH-2	CACAGAGAAGTTATCATCCAA
PolH-3	CCCGAGCATTTGGTGTCACTA
Ercc1-1	TACACGCAGGGTGGTATTATA
Ercc1-2	CACCGTGAAATCTGTGAACAA
Ercc1-3	CTCCTTAATAGTAGCCATCAA
Ercc4-1	CTGGTTCAAGTGGATGTGAAA
Ercc4-2	CACCGTGAAATCTGTGAACAA
Xrcc1-1	CCGGTGGATCTACAGTTGTAA
Xrcc1-2	TACACACAAGAGTTTAATAAA
Apex1-3	CCGAAAGTTTCTAAAGGACTT
RPL11-1	TCCAGCAGAAGTACGATGGAA
RPL11-2	CGGGAGTATGAGTTGCGGAAA
p21	CCAAAACAAAACAAACCTAAA
PTEN-1	CCAGATGTTAGTGACAATGAA
PTEN-2	AAGCTGAAAATTGTTACCTAA
PTEN-3	CAAGTTTAATGTTTAGTTCTA
Chk2*	CCCAGCCTTCTACTAGTCGAA

(*) denotes shRNA targeting human gene.

Supplementary Table S10: qRT-PCR primers used in this study.

	Forward	Reverse
Rev3	ACCAGCTCCTCCAGAAGTGA	ATGTCGGTCAAAGGAACCTG
PolH	GACAGGTGTCGCCTTGAAAT	CGGGCTTCATAGCTAACTGC
MSH2	CAGGTGGAAAACCACGAGTT	TGTTGTTGCGAAGCACTTTC
BRCA1	CCCTCAAGAAGCTGGAGATG	GCTGTAATGAGCTGGCATGA
BRCA2	CCAAAACTCAAGGAGGGTCA	GGAGAGTCAGCAGGCGTTAC
Ercc1	CCCTGAAAACAGGAGCAAAG	AGTCTGGATGGAGGTTGTGG
Ercc4	GCCGAATACTCGTGGTTGAT	ACAAAAAGGTTCCGCATCAC
Ercc8	GGACAACACCCTGGTGAACT	TAGGCTGGAACACACAGCAG
Xrcc1	GGGGGAAGAGTCAGAAGGAC	GGGGGTCTCACTGTCTGTGT
Apex1	GGAACAGGCAGACTCCATTC	GCTGCCCCCTTACTCTTCTT
RPL11	CTCCACCATGGCGCAAGAT	TTCTCCGGATGCCAAAGGAC
45S	ACACGCTGTCCTTTCCCTATTAACACTAAA	AGTAAAAAGAATAGGCTGGACAAGCAAAAC
Myc	ACACGGAGGAAAACGACAAG	AATTCAGGGATCTGGTCACG
Nedd9	GCCAATTCCCATCTGAAGAA	GTCGCTCAAACTCCTCCTTG
PTEN	TTTTTCTTCAGCCACAGGCTC	CTGTGCAACTCTGCAGTTAAA
Noxa	CCCAGATTGGGGACCTTAGT	AGTTATGTCCGGTGCACTCC
Puma	GCCCAGCAGCACTTAGAGTC	TGTCGATGCTGCTCTTCTTG
GAPDH	AGAACATCATCCCTGCATCC	CACATTGGGGGTAGGAACAC
Noxa*	AGGACTGTTCGTGTTCAGCTC	CTGCCGGAAGTTCAGTTTGTC
RPL11*	GAAGGGTCTAAAGGTGCGGG	ATGCTGAAACCTGGCCTACC
APC*	AAGCATGAAACCGGCTCACAT	CATTCGTGTAGTTGAACCCTGA
GAPDH*	GACAGTCAGCCGCATCTTCT	GCGCCCAATACGACCAAATC

Sequences are listed from 5' to 3'. (*) denotes sequence targeting human gene.